THESIS FOR THE DEGREE OF DOCTOR OF PHILOSOPHY

IN

THERMO AND FLUID DYNAMICS

Study of Supersonic Jet Noise Reduction using LES

by

Haukur Elvar Hafsteinsson

Department of Applied Mechanics
CHALMERS UNIVERSITY OF TECHNOLOGY
Göteborg, Sweden 2014

Study of Supersonic Jet Noise Reduction using LES
Haukur Elvar Hafsteinsson
ISBN 978-91-7597-086-8

Doktorsavhandlingar vid Chalmers tekniska högskola
Ny serie nr 3767
ISSN 0346-718X

Department of Applied Mechanics
Division of Fluid Dynamics
Chalmers University of Technology
SE-412 96 Göteborg
Sweden
Telephone +46-(0)31-7721000

This document was typeset using LaTeX

Printed at Chalmers Reproservice
Göteborg, Sweden, 2014

Study of Supersonic Jet Noise Reduction using LES

HAUKUR ELVAR HAFSTEINSSON

haukur.hafsteinsson@chalmers.se
Department of Applied Mechanics
Chalmers University of Technology

Abstract

Increases in air traffic and denser population around airports have led to stricter regulations on aircraft noise. High noise levels from high-speed aircraft can cause hearing damage in pilots and the airfield personnel. The engine is the main source of noise of all jet aircraft and is therefore a key component for improvement. Decreasing jet engine noise can in some cases reduce sonic fatigue and thereby increase the engine lifetime. In this thesis, the response of the radiated noise from a supersonic jet emitted from a converging diverging nozzle to steady-state, pulsed and flapping fluidic injection is studied using Large Eddy Simulation (LES), and comparisons are made with experimental data. An investigation is also presented in which actions were taken to reduce the internal shock strength by modifying the nozzle throat, and thereby reduce the radiated noise. The optimized nozzle nearly eliminates the internal shock, which reduces the double diamond structure in the jet plume but increases the strength of the shock at the nozzle exit. It has lower turbulence levels at the nozzle exit due to a weaker shock interaction with the shear layer. The optimized nozzle provides equal thrust to the sharp nozzle with 4 % less pressure without any acoustic penalty. The pulsed injection showed that the radiated noise is sensitive to the pulsation characteristics and the pulsation frequency. It was shown that the noise reduction with pulsed injection can equal the noise reduction of steady-state injection with a lower net mass flow of the pulsed injection. However, increased noise was noted at the downstream observers. The flapping injection cases that were investigated did not show improvements over the corresponding steady injection cases. These are positive findings, since steady injection should be simpler and more robust to apply to real jet engines. The injection was shown to impact the jet thrust, as expected. The net jet thrust increased with increased injection mass flow, whereas the specific thrust decreased. The momentum thrust was shown to decrease with increased injection mass flow whereas the pressure thrust increased due to a shock shift at the nozzle exit. The work presented in this thesis adds to the body of knowledge found in the literature about supersonic jet noise generation and its noise reduction using fluidic injection.

Keywords: CFD, LES, CAA, G3D, CD-nozzle, Supersonic Jet, Flow Control, Noise Reduction, Compressible Flow, PIV

List of Publications

This thesis is based on the work reported in the following papers:

Paper I H. Hafsteinsson, L.E. Eriksson, D. Cuppoletti, E. Gutmark and E. Prisell, *Active Suppression of Supersonic Jet Noise Using Pulsating Micro-Jets*, AIAA-2012-246, 50th AIAA Aerospace Sciences Meeting, Nashville, Tennessee, Jan. 9-12, 2012

Paper II H. Hafsteinsson, L.E. Eriksson, N. Andersson, D. Cuppoletti, E. Gutmark, *Noise Control of Supersonic Jet with Steady and Flapping Fluidic Injection*, Submitted to AIAA journal.

Paper III H. Hafsteinsson, N. Andersson, L.E. Eriksson, D. Cuppoletti, E. Gutmark, *LES Study of Screech Mechanism and the effect of Micro-Jet Injection*, Under consideration for publication in J. Fluid Mech.

Paper IV D. Cuppoletti, B. Malla, E. Gutmark, H. Hafsteinsson, L.E. Eriksson and E. Prisell, *The Response of Supersonic Jet Noise Components to Fluidic Injection Parameters*, AIAA-2013-2196, 19th AIAA/CEAS Aeroacoustics Conference, Berlin, Germany, May 27-29, 2013

Paper V D. Cuppoletti, E. Gutmark, H. Hafsteinsson, L.E. Eriksson and E. Prisell, *Analysis of Supersonic Jet Thrust with Fluidic Injection* AIAA 2014-0523, 52nd AIAA Aerospace Sciences Meeting, National Harbor, Maryland, January 13-17, 2014

Paper VI D. Cuppoletti, E. Gutmark, H. Hafsteinsson and L.E. Eriksson, *The Role of Nozzle Contour on Supersonic Jet Thrust and Acoustics*, AIAA Journal, 2014,1-21, doi: 10.2514/1.J052974

Paper VII H. Hafsteinsson, L.E. Eriksson, N. Andersson, P. Mora, E. Gutmark, and Prisell E., *Exploration of temperature effects on the far-field acoustic radiation from a supersonic jet*, AIAA 2014-2454, 20th AIAA/CEAS Aeroacoustics Conference, Atlanta, Georgia, June 16-20, 2014

Division of Work

Papers I-III and VII were written by H. Hafsteinsson and papers IV-VI were written by D. Cuppoletti. All LES was made by H. Hafsteinsson and all experiments were carried out by D. Cuppoletti except for the experimental results presented in paper VII that were conducted by P. Mora. Professor L.E. Eriksson helped with the implementation of the steady-state, pulsed and flapping mass flow boundary condition. The co-authors supervised and provided support during the writing process of all papers. Dr. B. Gustafsson carried out the optimization of the C-D nozzle presented in paper VI.

Other relevant publications

- R. Larusson , H. Hafsteinsson , N. Andersson and L.E. Eriksson, *Investigation of Supersonic Jet Flow Using Modal Decomposition*, AIAA 2014-3312, 20th AIAA/CEAS Aeroacoustics Conference, Atlanta, Georgia, June 16-20, 2014

- H. Hafsteinsson, L.E. Eriksson, N. Andersson, D. Cuppoletti, E. Gutmark and E. Prisell, *Near-Field and Far-Field Spectral Analysis of Supersonic Jet with and without Fluidic Injection*, AIAA 2014-1403, 52nd AIAA Aerospace Sciences Meeting, National Harbor, Maryland, January 13-17, 2014

- H. Hafsteinsson, L.E. Eriksson, N. Andersson, D. Cuppoletti, E. Gutmark, and E. Prisell, *Supersonic Jet Noise Reduction Using Steady Injection and Flapping Injection*, AIAA 2013-2144, 19th AIAA/CEAS Aeroacoustics Conference, Berlin, Germany, May 27-29, 2013

- D. Cuppoletti , E. Gutmark , H. Hafsteinsson , L.E. Eriksson and E. Prisell, *A Comprehensive Investigation of Pulsed Fluidic Injection for Active Control of Supersonic Jet Noise*, AIAA-2013-0009, 51st AIAA Aerospace Sciences Meeting, Grapevine Dallas/Ft. Worth Region, Texas, January 7-10, 2013

- D. Cuppoletti, E. Gutmark, B. Gustafsson, H. Hafsteinsson, L.E. Eriksson and E. Prisell, *Nozzle Throat Optimization on Acoustics and Performance of a Supersonic Jet*, AIAA-2012-2256, 18th AIAA/CEAS Aeroacoustics Conference, Colorado Springs, CO, June 4-6, 2012

- B. Gustafsson, D. Cuppoletti, E. Gutmark, H. Hafsteinsson, L.E. Eriksson and E. Prisell, *Nozzle Throat Optimization for Supersonic Jet Noise Reduction*, AIAA-2012-247, 50th AIAA Aerospace Sciences Meeting, Nashville, Tennessee, January 9-12, 2012

- H. Hafsteinsson, M. Burak, L.E. Eriksson and M. Billson, *Experimental and Numerical Investigation of a Novel Acoustic Liner Concept*, AIAA-2010-3770, 16th AIAA/CEAS Aeroacoustics Conference, Stockholm, Sweden, June 7-9, 2010

Acknowledgments

I want to thank my supervisor Professor Lars-Erik Eriksson for all his help and support during the work of this thesis. I would like to thank my predecessor Dr. Markus Burak, for introducing me to the meshing strategies of the G3D program, for showing me how to run the G3D solver and for providing me with the nozzle mesh. His work gave me a flying start to the thesis project. Furthermore, I wish to thank Dr. Niklas Andersson for his technical support while running the G3D solver and for his great patience and thorough help while proofreading all my writing. I also owe a great deal to my friends and colleagues at the Department of Applied Mechanics, Division of Fluid Mechanics, for creating a stimulating working atmosphere.

Morover, our partners, Professor Ephraim Gutmark, Dr. Daniel Cuppoletti and Pablo Mora at the University at Cincinnati are acknowledged for making it possible to validate the simulations with their high quality experimental data. I also want to thank them and all the friends I made during my stay as a visiting scholar at the Gas Dynamics and Propulsion Laboratory at UC for a very welcoming hospitality.

This work would not have been accomplished without financial support from FMV (Swedish Defence Materiel Administration). I also want to thank Chalmerska forskningsfonden and the Swedish American Foundation for making the visiting studies at UC a reality. In addition, the Swedish National Infrastructure for Computing (SNIC) is acknowledged for providing computer hours at C^3SE and NSC.

Finally, I would like to express my gratitude to my family for understanding my ambition to stay abroad while working on the thesis. Last but not least, Lára María, your constant support and encouragement throughout this work have been invaluable to me, thank you so much.

Nomenclature

Latin Symbols

c	speed of sound
C_{p}	specific heat at constant pressure
C_{v}	specific heat at constant volume
$C_{\mathrm{R}}, C_{\mathrm{I}}$	Smagorinsky model coefficients
e	energy
$\mathcal{F}_j$	Flux component
f	frequency
h	enthalpy
k	kinetic energy
n_i	Cartesian component of wall normal vector
p	pressure
M	Mach number
Pr	Prandtl number
q_j	energy diffusion vector
$\mathcal{Q}$	cell volume averaged state vector
Q	state vector in equaions on conservative form
R	gas constant
S_{ij}	strain rate tensor
T	Temperature
t	time
u_i	Cartesian components of velocity vector
U_{j}	jet-exit velocity
V	volume
x_i	Cartesian coordinate vector component

Greek Symbols

Δ	filter width

δ_{ij}	Kronecker delta tensor
ρ	density
μ	dynamic viscosity
ν	kinematic viscosity ($\nu = \mu/rho$)
σ_{ij}	viscous stress tensor
τ_{ij}	subgrid-scale stress tensor

Subscripts

0	total condition
t	turbulent quantity

Superscripts

$''$	unresolved quantity
$\tilde{}$	spatially Favre-filtered quantity
$-$	spatially filtered quantity

Abbrevations

BPR	bypass ratio
NPR	nozzle pressure ratio
NTR	nozzle temperature ratio
CAA	computational aeroacoustics
CFD	computational fluid dynamics
DNS	direct numerical simulation
LES	large eddy simulation
SGS	subgrid scale
MPI	message passing interface
(OA)SPL	(overall) sound pressure level
BBSN	broadband shock associated noise
TKE	turbulence kinetic energy

Contents

Chapter 1

Introduction

This work deals with numerical simulations for the prediction of supersonic jet noise with a focus on noise suppression using fluidic injection.

1.1 Importance of aircraft noise reduction

There has been a tremendous increase in air traffic ever since the first jet engine driven aircraft, the turbojet Heinkel He 178 prototype of the German Air Force, took off in the 1940s. Aircraft are noisy, and acoustic loads can lead to hearing damage or high blood pressure among the aircraft crew and the airfield personnel. High cock-pit noise levels also interfere with speech communication and can therefore cause safety problems.The amount of damage a noise can cause depends on individual sensitivity to the amplitude and the frequency of the sound waves and the exposure time. The National Institute for Occupational Safety and Health (NIOSH) has issued standards for recommended noise exposure limits, as illustrated in Fig 1.1.

An increment of 3 dBA corresponds to a doubling of the sound intensity. This means that, if the noise levels are increased by 3 dBA, the exposure time needs to be halved to maintain the same risk of hearing damage. Current UK legislation quotes an allowable daily noise dose for a nominal 8-hour working day of 85 dBA. Considering cock-pit noise levels of typical military jet aircraft [2], the noise exposure is far above the 8-hour limit even though the pilot uses modern passive helmet attenuation. For example, the mean noise dose received by the pilot in a Harrier GR5 at high-speed, low level flight is 96.9 dBA. This means that allowable daily flying is 31 minutes in the 85 dBA limit and only 9.8 minutes if the limit is decreased to 80 dBA. Table 1.1 shows further examples of cock-pit noise levels in military jet aircraft.

Not only aircraft personnel suffer. Experiments show that people living in areas frequently exposed to low-altitude flight noise are in danger of long-term health risks [3]. The intense effects of low-altitude flight noise can be related to

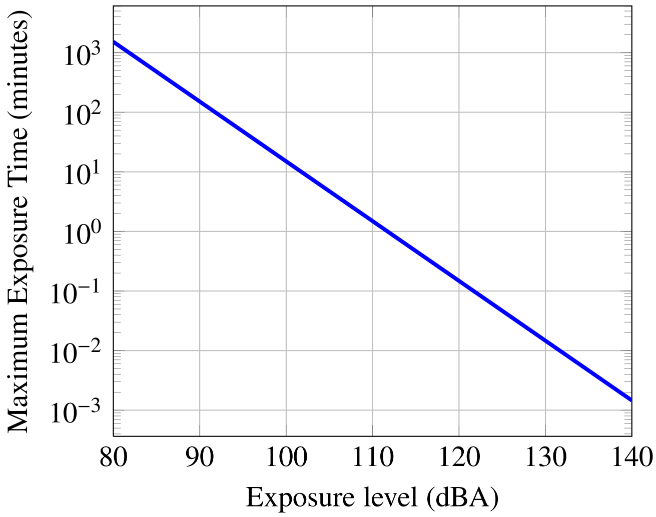

Figure 1.1: Recommended noise exposure limit by the National Institute for Occupational Safety and Health (NIOSH) [1].

Table 1.1: Measured noise dose received by pilot and corresponding allowable flying duration in accordance with legislation. The data are taken from [2].

Aircraft	**Mean dose + 2 SD (dBA)**	**Allowable daily flying minutes**	
		85 dBA limit	**80 dBA limit**
Hawk	96.2	36.4	11.5
Harrier GR5	96.9	31.0	9.8
Jaguar GR1	101.0	12.1	3.8

its physical characteristics, which are different from other noise sources in our environment. The very high sound level and the very rapid increase is unique to this type of noise. The maximal sound levels of the most frequent overflights are in the range of 100 to 115 dBA, although higher levels of up to 125 dBA occur but much less often. The increase rate is also very high, 75 dB/s and even higher increase rates of 200 dB/s have been measured. In addition to the high noise around the airfields, the trends of increased population around airfields in the past decades has resulted in higher demands for lower noise emitting aircraft with stricter regulations on noise. Furthermore, it is not only humans and other living beings that are harmed by aircraft noise. Acoustic load can also cause sonic fatigue in the aircraft structure [4, 5] and, if the load is sustained with considerable acoustical energy under sufficiently long periods of time, it can cause the structure to break with possibly serious consequences.

1.2 Aircraft noise sources

The main noise sources of existing modern aircraft depends on the type of aircraft. The size, the shape and the propulsion system of an aircraft are adapted to its particular purpose of use. Ranked from low noise emitting transport to high noise transport, the main aircraft categories are the following; general aviation (GA), helicopters, short take-off and landing (STOL), conventional take-off and landing (CTOL), supersonic transport (SST) and hypersonic transport (HST) [6]. The main noise source common to those groups is the powerplant.

1.2.1 Powerplant

There are two main categories of modern jet engines. The first type is the pure jet single shaft engine originally designed in the 1950's and used in the Comet, the Caravelle and the early B707 and DC8. Since then, the power and efficiency of these engines have increased substantially, and they are commonly used in today's high speed supersonic jet aircraft. The main part of the air entering the engine inlet is transported through the compressor, the combustion chamber and the nozzle, and it exits the engine exhaust at velocities up to 700 m/s. The second type is the two or three shaft turbofan jet engine. It was originally designed in the 1970s and 1980s and is currently used in today's civil aircraft. In turbofan engines, only part of the air entering the air intake passes through the core. The rest of the air enters the bypass duct. A higher bypass ratio, typically around 20:1, increases the efficiency of the jet-engine and makes it possible to reduce the exit velocity with maintained thrust. A typical exit velocity of the hot jet is around 400-500 m/s. The major noise sources of those two types of jet engines are the compressor, the turbine and the jet. Of those three, the jet noise is the dominant noise source at take-off. In the by-pass type of engine, a rotor-stator interaction in the by-pass duct is another source of noise, called fan noise. For high-bypass ratio engines, the fan exhaust noise is of the same magnitude or higher than the jet exhaust noise at take-off, as shown in Fig. 1.2.

Jet Noise

Jet noise arises from the mixing process between the exhaust flow and the atmosphere, as well as from internal mixing. The mixing process is driven by the temperature, pressure and velocity gradients between the flow and its surroundings. Mixing noise and shock-associated noise are the two main acoustic signatures of jet noise; the latter arises only in supersonic flows, as the name indicates. Mixing noise originates from shear stress fluctuations in the jet plume and has a broadband spectrum because of the wide range of length scales existing in the flow field. Crow and Champagne [8] found that the large turbulence structures and the fine-scale turbulence are important noise sources in jet flow.

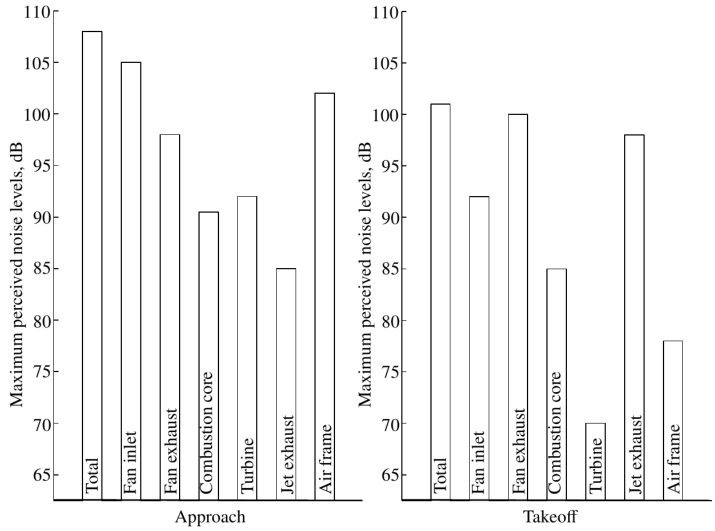

Figure 1.2: Noise sources of a typical by-pass engine. Reproduced from [7].

The sound intensity of jet flow varies with the eighth power of the jet velocity, $I \propto U^8$ [9], except for high velocities well above the supersonic limit where the sound intensity starts to vary with the jet speed to the power of three, $I \propto U^3$ [10]. This means for example that the reduced velocity of high bypass ratio engines, where the exit velocity is halved compared to no or low bypass ratio engines, results in reduced sound intensity by some 21 dB [11].

An interesting phenomenon in subsonic jets is the so-called “cone of silence” [12]. The term draws its name from the noise directivity in subsonic jets. Noise sources appearing in the jet plume radiate sound waves that are convected downstream by the jet flow. However, since the jet mean axial velocity decreases in the radial direction, the convection speed differs depending on the radial location of the noise source. The radiated sound waves are therefore refracted outward as they travel downstream. This results in lower noise in a conical sector for the downstream observers. Measurements have shown up to a 20 dB noise reduction in the presence of a cone of silence [13]. This phenomenon, however, does not exist in supersonic jets due to the different noise generation mechanism. The reason for a non existing cone of silence is related to the location of the noise sources generated by the large turbulence structures. The large turbulence structures are a dominant noise source in the downstream direction, typically up to 60° measured from the flow direction. Since the large scale turbulence mixing noise is mainly generated in the outer shear layer, where the supersonic core flow meets the surrounding subsonic flow, no refraction occurs and hence there is no cone of silence in supersonic jets.

Tam [14] suggested that the large structures can be thought of as a collection of instability waves, each having a varying frequency, amplitude and phase velocity.

As each instability wave convects downstream with the flow, it interacts with the jet surroundings. If the phase velocity is supersonic, then the interaction results in the generation of an intense noise radiation in the form of Mach waves, which are infinitesimally weak oblique shocks. The frequency, phase velocity and amplitude of the instability wave determine the angle of the Mach wave, i.e. the directivity of the noise. Because of the variation of the instability waves, the noise is radiated in different directions, mainly lower than 60° from the flow direction, as shown in Fig. 1.3 For higher angles the sound pressure levels decrease and reach a certain minimum background noise, which is thought to be generated by the fine scale turbulence.

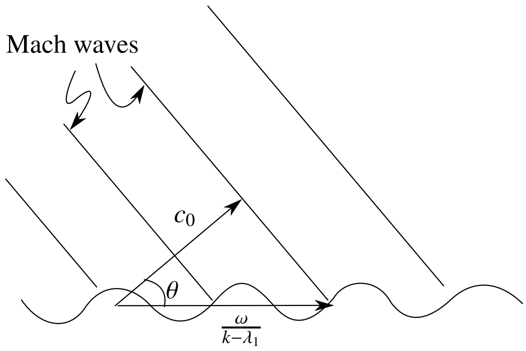

Figure 1.3: Mach wave radiation due to a supersonic traveling wave component. Adapted from Tam [15]

Broadband shock associated noise and screech tone noise are additional noise sources in addition to the mixing noise in supersonic jets. In contrast to the mixing noise, these are only generated in the presence of a quasi-periodic shock cell structure in the jet plume. The broadband shock associated noise is generated by the interaction of the downstream propagating large turbulence structures/instability waves and the quasi-periodic shock cell structure. In contrast to the mixing noise caused by large scale structures, broadband shock associated noise is mainly prominent in the upstream directions. The broadband shock associated noise is observed, as the name indicates, a broad peak in the noise spectra. The peak is the dominant noise component for the upstream observers and disappears into the mixing noise for the downstream angles. It is worth mentioning that the peak's center shifts to higher frequencies, and the half-width increases, as the observer angle measured from the flow direction decreases. This is a general behavior of the broadband shock associated noise that appears in imperfectly expanded supersonic jets.

Harper-Bourne [16] derived a relation for the peak frequency of the shock-associated noise, at a given observer angle, assuming an array of monopole noise sources located at the tip of the shocks in the shear-layer. The noise sources are driven by the interaction of the tipping shocks and the convected eddies in the

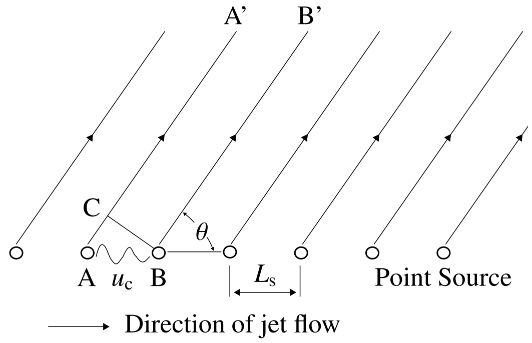

Figure 1.4: Schematic of the phased point-source array model. Adapted from Tam [15]

shear layer. The key identification made by Harper-Bourne was the phase-lag between the sources driven by the eddy convection correlated by the time it takes the turbulence to convect from one point source to another (see Fig. 1.4). If L_s is the shock cell spacing and u_c the convection velocity, then the time taken for turbulence to be convected from point source A to point source B is $T_{AB} = L_s/U_c$. Thus, the time delay between point source A and point source B is T_{AB}. By definition, the noise radiates evenly in all directions at each point source. Considering one specific direction, θ, it is clear that path AA' is longer than BB'. The time it takes a sound wave to travel the extra distance is $T_{AC} = L_s \cos\theta/c$, where c is the ambient speed of sound. Therefore, the two sound waves are generally out of phase with each other when they arrive at an observer in the far-field. However, if certain criteria are met, there is a possibility of a maximum constructive reinforcement of the sound intensity. The condition for maximum wave superposition does occur when the difference between the turbulence convection time, T_{AB}, and the sound propagation time, T_{AC}, is equal to an integer multiple of the wave period. This happens when $T_{AB} - T_{AC} = n/f_p$:

$$\left(\frac{L_s}{U_c} - \frac{L_s\cos\theta}{c}\right) = \frac{n}{f_p} \qquad (n = 1, 2, ...) \tag{1.1}$$

and the primary peak frequency, f_p corresponds to the case of $n = 1$,

$$f_p = \frac{U_c}{L(1 - M_c\cos\theta)} \tag{1.2}$$

In contrast, Tam [15, 17] used another approach to arrive to the same relation. Tam hypothesized that the quasi-periodic shock cell structure can be considered as a superposition of time-independent waveguides or Fourier modes of the mean flow of the jet. Each mode corresponds to a different wavelength, and each of them scatters noise in different direction upon perturbation. Furthermore, the large scale turbulence structures, that interact with the shocks, are random and consist of wave-like components of a fairly broad range of frequencies. As a result, the principal direction of the noise radiation is different from one mode to another, and the far-field spectra is a superposition from the collection of different modes.

The third noise source component in supersonic jets is screech tone noise. It was first observed by Powell in 1953 [18]. The screech tone noise is thought to be created through an acoustic feedback loop. The general idea is as follows: at the nozzle exit, where the shear layer is the thinnest, a large velocity gradient causes the generation of instability waves. These waves grow quickly in magnitude and, when large enough, start to interact with the shock cell structure, typically after four or five shock cells downstream of the nozzle exit. The interaction causes sound waves to be emitted upstream in the same fashion as the broadband shock associated noise. As the sound waves travel upstream, they will reach the nozzle exit, where they excite more instability waves as they pass the nozzle lip. In this way, the feedback loop is closed. Screech is radiated mainly in the upstream direction and can be thought of as a special case of the broadband shock associated noise. It has been shown that a reasonable estimate of the screech tone frequency is obtained by setting $\theta = 180^\circ$ in Eqn. 1.2 and is therefore a lower bound of the frequency of the shock associated noise. However, in contrast, the frequency of the screech tone is independent of the observer angle. The intensity of the screech tone is affected primarily by the jet Mach number, the jet temperature, the nozzle lip thickness and the presence of sound reflecting surfaces near the nozzle exit. Fortunately, the screech intensity decreases with jet temperature and is therefore generally not considered hazardous by engineers as a potential cause of sonic fatigue in jet engines.

1.3 Noise reduction devices

Extensive effort has been made in noise reduction of jet engines since the 1960s when commercial flights started. Demands for reduced noise strongly increased in the 1970s, at which stricter regulations for maximum allowed radiated noise were set [11]. The highest priority was given to jet noise since it was, at that time, the main noise source. Second came fan noise, which had been increasing with larger fan size with the high bypass ratio jet engines. Although theoretical tools for predicting jet noise became available from the research done in the 1950s and the 1960s, those tools were not helpful for predicting the suppression of additional noise reduction devices. Therefore, most of the ideas proposed had to be tested experimentally. The main focus was on reducing the potential core of the jet and/or breaking down the shock cell structure in the jet plume. A less powerful shock cell structure would reduce the broadband shock associated noise. Reducing the potential core could be done by increasing the mixing between the jet and its surroundings. Increased mixing could also break down the large structures in the jet to smaller structures, which should result in higher frequency noise, hopefully above the frequency range at which the human ear is the most sensitive

($>$ 4.0 kHz). Higher frequencies are absorbed better by the atmosphere and do not propagate as far as lower frequencies. Hence, the idea of so called mixing devices became popular. However, with decreased noise of the mixing devices, there is a penalty of decreased efficiency and therefore higher fuel consumption. Early noise suppression devices had about a 2-3 % increase in fuel burn for a peak angle noise reduction of about 5-8 PNdB and the penalty increased drastically with further suppression of noise. There is thus a need of noise suppression devices that have a high reduction with as low a penalty as possible. However, this is hard to achieve with the permanently installed mixing devices that were developed during that period, such as the chevron, chute, corrugated or lobed nozzle, since they all tend to introduce losses in the system. Thus came the idea of using fluidic injection into the jet flow. It was shown that micro-jets are a promising technique for an active noise suppression device that can gain similar or even better noise reduction than passive mixing devices such as chevrons. With an active devices such as the micro-jet injection, there is a possibility to turn on the injection only when needed, for example at take-off and landing, and thereby limit the losses of the total flight. However, the mass flow needed for the injection is bled from the compressor, which will lose performance when there is too high a bleeding rate. It is therefore important to keep the injection mass flow rate as low as possible.

1.3.1 Fluidic injection

A thorough review of fluidic injection research for jet noise reduction applications in the past 50 years is given by Henderson [19]. Early research on fluidic injection was mainly experimental, using aqueous injection. However, for practical reasons, water injection is not considered an optimal injection fluid since extra weight is added to the aircraft that needs to be carried during flight. Air, which could be bled from the compressor when needed, is thus considered a more appealing option. In the past decade, research using gaseous injection has gained momentum and increased CPU power has opened doors for computational jet noise predictions with fluidic injection [20, 21, 22, 23, 24, 25].

To the author's knowledge, there is a limited amount of published work on transient fluidic injection applied to supersonic jets for noise reduction, especially for numerical simulations. A brief overview is given below of published work on transient injection intended to reduce the radiated noise of free jets.

Raman and Chain [26] gave an overview of today's innovative actuators that are used for flow control. These are the synthetic jet actuators, piezoelectric actuators, resonance tube actuators and fluidic actuators. So–called plasma actuators have also been applied for flow control. In practical applications, the frequency limit of fluidic actuators is usually below 500 Hz which is considered to be in the low frequency range.

Ragaller *et al.*[27] made measurements of the radiated noise from a supersonic jet (M=1.8). The jet was subjected to a pulsed micro-jet trailing-edge water injection. Their approach was to investigate low frequency injection, i.e. 1 Hz and 10 Hz at duty cycles of 50% and 75%, where 100% duty cycle corresponds to a steady-state injection. Their main finding was that the noise reduction of the pulsed injection approached the noise reduction of the steady-state injection when the duty cycle was increased.

Huet *et al.*[28] made LES simulations on a 50 mm single-stream high-speed (M=0.9) nozzle with both steady-state and pulsed micro-jet air injection. They used 12 trailing edge micro-jets with an injection angle of 45 degrees to the jet axis. Two injection frequencies were tested ($f = 3.0$ kHz and $f = 9.0$ kHz, which correspond to Strouhal numbers of $St = 0.5$ and $St = 1.5$, respectively). They observed a significant noise reduction over the whole frequency range with pulsed injection. Furthermore, the pulsed injection resulted in a greater noise reduction as compared to steady-state injection for both injection frequencies. However, an increased tonal noise at the forcing frequency and its harmonics was observed. Although an understanding of the reaction of subsonic jets to pulsed injection is of great interest, a pulsed injection to supersonic jets is more relevant to the work presented in this thesis.

Krothapalli *et al.*[29] conducted an experimental investigation of the radiated noise of a high temperature (1033 K) supersonic jet (M=1.38) with a nozzle exit diameter of 50.8 mm. Both steady-state and pulsed internal injection, with an injection frequency of 2000 Hz using 4 actuators, were applied. However, the results showed little or no effect on the radiated noise.

An extensive study was recently done on plasma actuators for high speed and high Reynolds number subsonic [30, 31, 32] and supersonic [33, 34, 35, 36] jet mixing and noise reduction. The benefit of using plasma actuators is the very high frequency operating level (200 kHz). Samimy *et al.*[33] carried out experiments on the effect of azimuthal modes at different injection frequencies on the radiated noise from a perfectly-expanded supersonic (M=1.3) axi-symmetric heated and unheated jet. It was observed that a higher azimuthal mode (m=3) resulted in a lower tone noise increment at the forcing frequency, compared to an axi-symmetric pulsation (m=0). The effect of azimuthal injection modes was further investigated by Kearney-Fischer and Samimy [34] for different Strouhal numbers and jet temperature ratios. They observed that Strouhal numbers higher than $St = 1.5$ were needed for reduced noise radiation. This result indicates that an additional reduction of the radiated noise can be achieved with higher injection frequencies compared to the pulsed cases presented in paper I, where Strouhal numbers up to 0.8 were investigated.

1.3.2 Jets in crossflow

The flow mechanism of transverse/oblique jets in crossflow has been widely studied in the past for various applications, for example enhanced fuel efficiency [37], film cooling [38] and jet noise reduction [39, 40]. The complex three dimensional flow pattern of an underexpanded transverse jet in supersonic crossflow is illustrated in Fig.1.5. A bow-shock is formed upstream of the injector and the flow separates upstream of the bow-shock. A recirculation zone, surrounded by a horse-shoe vortex, is created downstream of the injector. A normal shock (Mach disk) is formed at a short distance from the underexpanded transverse jet exhaust, and it leans towards the direction of the crossflow. With increased injection pressure, the angle of the normal shocks decreases and finally aligns with the nozzle wall at sufficiently high pressure ratios. The injector penetration has been shown to be dependent on the jet-to-freestream momentum flux ratio defined as follows:

$$J = \frac{(\rho u^2)_\mathrm{i}}{(\rho u^2)_\mathrm{j}} \tag{1.3}$$

Further, injector penetration has been shown to decrease with increased angle from the transverse direction which is logical since the transverse momentum thrust is lower.

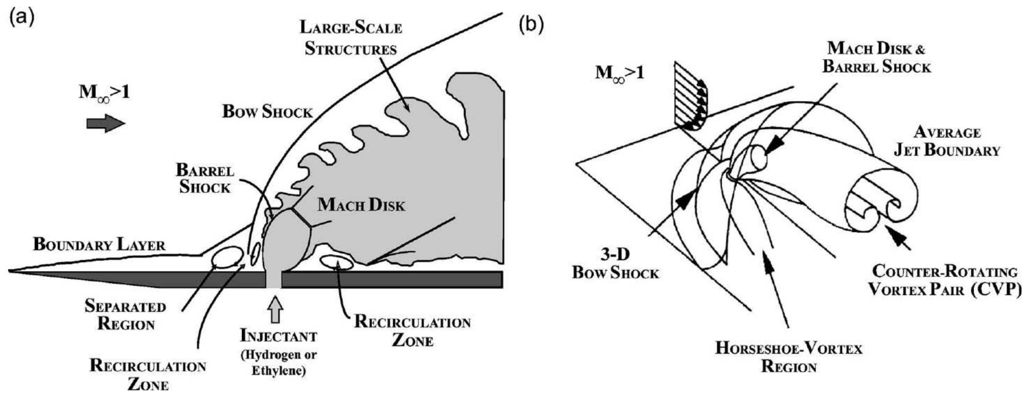

Figure 1.5: Schematic of underexpanded jet injected to a supersonic cross flow. a) Side view of instantaneous flow [37], b) Perspective view of time-averaged flow [41]

Gutmark *et al.*[42] showed that the shape of the injector cross-sectional area affects the penetration, mixing characteristics and structure of a subsonic transverse jet in subsonic crossflow. Different aspect ratios of the cross-sectional area was tested (long and thin). Aligning the longer edge of the injector with the flow direction caused the maximum penetration, the smallest recirculation area downstream of the injector and the least jet spreading. It is reasonable to assume that the same holds for jets in supersonic crossflows.

Chapter 2

Methodology

Large-Eddy Simulations are used in this thesis as a numerical tool to obtain the jet flow. LES provides more accurate results of the flow-field as compared to the less computationally expensive URANS. Both approaches solve the Navier-Stokes equations. The main difference is that URANS is based on time averaging while LES is based on spatial averaging. In URANS, all length scales are modelled, while, in LES, only the small scales are modelled and the large scales are resolved. In the present work, the limit of the resolved scales is specified as the smallest cell size. The smaller the cell size, the more LES starts to approach direct numerical simulations (DNS), where all scales are resolved. However, DNS is today considered to be a too computationally expensive method for most industrial applications and LES is therefore still a more feasible option.

2.1 Governing equations

In this thesis, the compressible form of the Navier-Stokes equations is applied to solve the fluid flow. The equations were established by Claude-Louis Navier and George Gabriel Stokes where Newton's viscosity law and Fourier's heat law are used to account for the viscous stresses and the heat flux, respectively. They consist of the continuity, the momentum and the energy equations:

$$\frac{\partial \rho}{\partial t} + \frac{\partial (\rho u_i)}{\partial x_i} = 0 \tag{2.1}$$

$$\frac{\partial (\rho u_i)}{\partial t} + \frac{\partial (\rho u_i u_j)}{\partial x_j} = -\frac{\partial p}{\partial x_i} + \frac{\partial \sigma_{ij}}{\partial x_j} \tag{2.2}$$

$$\frac{\partial (\rho e_0)}{\partial t} + \frac{\partial \left(\rho e_0 u_j\right)}{\partial x_j} = -\frac{\partial p u_j}{\partial x_j} + \frac{\partial}{\partial x_j}\left(C_{\mathrm{p}} \frac{\mu}{Pr} \frac{\partial T}{\partial x_j}\right) + \frac{\partial}{\partial x_j}\left(u_i \sigma_{ij}\right) \tag{2.3}$$

where the viscous stress σ_{ij} in Eqn. 2.2 and Eqn. 2.3 is defined by

$$\sigma_{ij} = \mu\left(2S_{ij} - \frac{2}{3}S_{mm}\delta_{ij}\right) \tag{2.4}$$

and the strain-rate tensor, S_{ij}, is given by

$$S_{ij} = \frac{1}{2}\left(\frac{\partial u_i}{\partial x_j} + \frac{\partial u_j}{\partial x_i}\right) \tag{2.5}$$

Pr in Eqn. 2.3 is the Prandtl number specified by

$$Pr = \frac{\mu C_{\mathrm{p}}}{k} \tag{2.6}$$

where C_{p} is the specific heat at constant pressure and μ is the viscosity. Both C_{p} and μ are assumed to be constant. This means that the gas is considered to be calorically perfect, i.e. the internal energy and the enthalpy are linear functions of temperature.

$$\begin{aligned} e &= C_{\mathrm{v}}T \\ h &= C_{\mathrm{p}}T \\ C_{\mathrm{v}} &= C_{\mathrm{p}} - R \end{aligned} \tag{2.7}$$

Furthermore, the system of governing equations, Eqns. 2.1-2.3 is closed by assuming that the gas is thermodynamically perfect, i.e. it follows the gas law

$$p = \rho RT \tag{2.8}$$

2.2 Spatial Filtering

A low-pass spatial filter is applied to the governing equations in order to remove the small scales of the flow while resolving the large scales. The small scales are filtered out using an externally specified filter width. A box filtering is applied in the work presented here, i.e. the filter width is locally coupled to the discretization in the finite-volume solver. Since the small scale features are filtered out they need to be modeled using a subgrid scale model.

2.2.1 Favre Filtering

The LES simulations presented in this thesis are based on a spatial Favre filtering. This is a mass weighted spatial filter that is commonly applied in compressible flows. The flow properties are decomposed using Favre filtering as follows:

$$\Phi = \tilde{\Phi} + \Phi'' \tag{2.9}$$

Here, $\Phi^{''}$ is the unresolved part of Φ, and $\tilde{\Phi}$ is the Favre filtered resolved part which is obtained as follows

$$\tilde{\Phi} = \frac{\overline{\rho\Phi}}{\overline{\rho}} \tag{2.10}$$

By applying the Favre filtering operator from Eqn. 2.10 to the Navier-Stokes equations, i.e. Eqns. 2.1-2.3, they can be written as

$$\frac{\partial\overline{\rho}}{\partial t} + \frac{\partial(\overline{\rho}\tilde{u}_i)}{\partial x_i} = 0 \tag{2.11}$$

$$\frac{\partial(\overline{\rho}\tilde{u}_i)}{\partial t} + \frac{\partial(\overline{\rho}\tilde{u}_i\tilde{u}_j)}{\partial x_j} = -\frac{\partial\overline{p}}{\partial x_i} + \frac{\partial\overline{\sigma}_{ij}}{\partial x_j} + \frac{\partial\tau_{ij}}{\partial x_j} \tag{2.12}$$

$$\begin{aligned}\frac{\partial\left(\overline{\rho}\tilde{e}_0\right)}{\partial t} + \frac{\partial\left(\overline{\rho}\tilde{e}_0\tilde{u}_j\right)}{\partial x_j} = &-\frac{\partial\overline{p}\tilde{u}_j}{\partial x_j} + \frac{\partial}{\partial x_j}\left(C_{\mathrm{p}}\frac{\mu}{Pr}\frac{\partial\tilde{T}}{\partial x_j} + q_j^{SGS}\right) + \frac{\partial}{\partial x_j}\left(\overline{u_i\sigma_{ij}}\right)\\ &-\frac{1}{2}\frac{\partial}{\partial x_j}\overline{\rho}\left(\widetilde{u_iu_iu_j} - \widetilde{u_iu_i}\tilde{u}_j\right)\end{aligned} \tag{2.13}$$

The Favre filtered viscous stress tensor is as follows

$$\overline{\sigma}_{ij} = \mu\left(2\tilde{S}_{ij} - \frac{2}{3}\tilde{S}_{mm}\delta_{ij}\right) \tag{2.14}$$

and the Favre filtered strain rate tensor is the following

$$\tilde{S}_{ij} = \frac{1}{2}\left(\frac{\partial\tilde{u}_i}{\partial x_j} + \frac{\partial\tilde{u}_j}{\partial x_i}\right) \tag{2.15}$$

Comparison of the Navier-Stokes equation with and without Favre-filtering, i.e. Eqns. 2.1-2.3 and Eqns. 2.11-2.13, shows that the form of the Favre-filtered equations is very similar to the unfiltered equations. However, an extra term appears in the Favre-filtered momentum equation. This is the subgrid-scale viscous stress tensor, given by

$$\begin{aligned}\tau_{ij} &= -\overline{\rho}\left(\widetilde{u_iu_j} - \tilde{u}_i\tilde{u}_j\right)\\ &= -\overline{\rho}\left(\underbrace{\left(\widetilde{\tilde{u}_i\tilde{u}_j} - \tilde{u}_i\tilde{u}_j\right)}_{I} + \underbrace{\left(\widetilde{u_i^{''}\tilde{u}_j} + \widetilde{\tilde{u}_iu_j^{''}}\right)}_{II} + \underbrace{\widetilde{u_i^{''}u_j^{''}}}_{III}\right)\end{aligned} \tag{2.16}$$

Terms $I - III$ are often referred to as Leonard stress, cross stress and subgrid-scale Reynolds stress, respectively. Furthermore, a term analogous to the subgrid-scale viscous stress tensor appears in the Favre-filtered energy equation. This term is denoted as the subgrid-scale heat flux term and is given by

$$\begin{aligned}q_j^{SGS} &= -C_{\mathrm{p}}\overline{\rho}\left(\widetilde{Tu_j} - \tilde{T}\tilde{u}_j\right)\\ &= -C_{\mathrm{p}}\overline{\rho}\left(\widetilde{\tilde{T}\tilde{u}_j} - \tilde{T}\tilde{u}_j + \widetilde{T^{''}\tilde{u}_j} + \widetilde{\tilde{T}u_j^{''}} + \widetilde{T^{''}u_j^{''}}\right)\end{aligned} \tag{2.17}$$

The second to last term in the energy equation, i.e. the product $(\overline{u_i \sigma_{ij}})$, is replaced with $(\tilde{u}_i(\overline{\sigma}_{ij} + \tau_{ij}))$. Moreover, the last term of the energy equation is considered negligible. This means that there are only two unknown terms that need to be modelled, i.e. the subgrid-scale viscous stress tensor, τ_{ij}, and the subgrid-scale heat flux term, q_j^{SGS}, from the Favre-filtered momentum and energy equations, respectively.

2.3 Subgrid-Scale Model

In high Reynolds number turbulent flows, the large energy containing eddies take energy from the mean flow and transfer it to smaller scales. The smaller scales are activated and further transfer energy to even smaller scales. This process continues until the scales are small enough to be dissipated by the viscous forces of the fluid. As shown in the previous section, the LES does not resolve the small scales and they therefore need to be modelled. The most widely used subgrid-scale model is the Smagorinsky model [43], which is of an eddy-viscosity type and appears as follows:

$$\tau_{ij} - \frac{1}{3}\tau_{mm}\delta_{ij} = -2\nu_{\mathrm{t}}\overline{S}_{ij} \tag{2.18}$$

This assumes that the energy of the large eddies is in equilibrium with the dissipation, i.e. no energy is lost during the cascade process. The turbulent eddy viscosity is given by

$$\nu_{\mathrm{t}} = (C_{\mathrm{s}}\Delta)^2 \left|\overline{S}\right| \tag{2.19}$$

where C_{s} is the Smagorinsky constant.

The subgrid-scale model used in the present work is the Smagorinsky part of the model proposed by Erlebacher *et. al* [44] for compressible flows and is based on Favre-filtered quantities. The subgrid-scale viscous stress tensor from Eqn. 2.16, is modelled as follows:

$$\tau_{ij} = \mu_{\mathrm{t}}\left(2\tilde{S}_{ij} - \frac{2}{3}\tilde{S}_{mm}\delta_{ij}\right) - \frac{2}{3}\overline{\rho}k^{SGS}\delta_{ij} \tag{2.20}$$

where the subgrid-scale kinetic energy, k^{SGS}, is defined as

$$k^{SGS} = C_{\mathrm{I}}\Delta^2\tilde{S}_{mn}\tilde{S}_{mn} \tag{2.21}$$

and μ_{t}, the subgrid-scale dynamic viscosity, is given by

$$\mu_{\mathrm{t}} = C_{\mathrm{R}}\overline{\rho}\Delta^2\sqrt{\tilde{S}_{mn}\tilde{S}_{mn}} \tag{2.22}$$

The constants C_{R} and C_{I} are the Smagorinsky model constants, here given by

$$\left\{\begin{array}{lcl} C_{\mathrm{R}} & = & 0.012 \\ C_{\mathrm{I}} & = & 0.0066 \end{array}\right. \tag{2.23}$$

The filter width, Δ, appearing in Eqns. 2.21 and 2.22 is specified as the minimum of the local grid cell, i.e. $\Delta = \min(\Delta_1, \Delta_2, \Delta_3)$, which was successfully used by Anderson [45] and Burak [46]. Finally, the subgrid heat flux appearing in Eqn. 2.17 is modelled by applying a temperature gradient formulation

$$q_j^{SGS} = C_\mathrm{p} \frac{\mu_\mathrm{t}}{Pr_\mathrm{t}} \frac{\partial \tilde{T}}{\partial x_j} \tag{2.24}$$

2.4 Numerical Method

The code used in the simulations presented in this thesis is a finite volume solver in the G3D family of codes originally developed by Eriksson [47]. It solves the compressible flow equations in conservative form on a boundary-fitted, curvilinear, non-orthogonal multi-block mesh. The code was implemented for parallel computations using a Message Passing Interface (MPI) to tackle flow problems with a large number of computational nodes within a reasonable time frame. The code has been used with good results for many applications, for example: LES of free shear flows by Mårtensson *et al.*[48], subsonic jet flows by Andersson [45], shock/shear-layer interaction by Wollblad [49] and supersonic jet flows by Burak [46].

The finite volume method is a numerical approach for solving partial differential equations, e.g. compressible flow equations. In short, the equations under consideration are integrated over the computational domain. The computational domain is split into smaller sub-volumes, and the flow variables are obtained at the center of each volume. This procedure is described below. For convenience, the Favre-filtered Navier-Stokes equations are written in a more compact form

$$\frac{\partial Q}{\partial t} + \frac{\partial \mathcal{F}_j}{\partial x_j} = 0 \tag{2.25}$$

where

$$Q = \begin{bmatrix} \overline{\rho} \\ \overline{\rho}\tilde{u}_i \\ \overline{\rho}\tilde{e}_0 \end{bmatrix} \tag{2.26}$$

and

$$\mathcal{F}_j = \begin{bmatrix} \overline{\rho}\tilde{u}_j \\ \overline{\rho}\tilde{u}_i\tilde{u}_j + \overline{p}\delta_{ij} - \overline{\sigma}_{ij} - \tau_{ij} \\ \overline{\rho}\tilde{e}_0\tilde{u}_j + \overline{p}\tilde{u}_j - C_\mathrm{p}\left(\left(\frac{\mu}{Pr} + \frac{\mu_t}{Pr_t}\right)\frac{\partial \tilde{T}}{\partial x_j}\right) - \tilde{u}_i\left(\overline{\sigma}_{ij} + \tau_{ij}\right) \end{bmatrix} \tag{2.27}$$

The total flux, $\mathcal{F}_j$, is divided into a convective part and a diffusive part as follows

$$\mathcal{F}_j = \begin{bmatrix} \overline{\rho}\tilde{u}_j \\ \overline{\rho}\tilde{u}_i\tilde{u}_j + \overline{p}\delta_{ij} \\ \overline{\rho}\tilde{e}_0\tilde{u}_j + \overline{p}\tilde{u}_j \end{bmatrix} + \begin{bmatrix} 0 \\ -\overline{\sigma}_{ij} - \tau_{ij} \\ -C_\mathrm{p}\left(\left(\frac{\mu}{Pr} + \frac{\mu_t}{Pr_t}\right)\frac{\partial \tilde{T}}{\partial x_j}\right) - \tilde{u}_i\left(\overline{\sigma}_{ij} + \tau_{ij}\right) \end{bmatrix} \tag{2.28}$$

Eqn.2.25 is integrated over an arbitrary volume as follows

$$\int_{\Omega} \frac{\partial Q}{\partial t} dV + \int_{\Omega} \frac{\partial \mathcal{F}_j}{\partial x_j} dV = 0 \tag{2.29}$$

Introducing Q as the volume average over each cell gives

$$\int_{\Omega} \frac{\partial Q}{\partial t} dV = \frac{\partial Q}{\partial t} V \tag{2.30}$$

where V is the volume of the cell. Converting the divergence term of the second volume integral to a surface integral using Gauss theorem gives

$$\int_{\Omega} \frac{\partial \mathcal{F}_j}{\partial x_j} dV = \int_{\partial\Omega} \mathcal{F}_j \cdot d\mathcal{S}_j \tag{2.31}$$

The flux integral is approximated by using the area multiplied by the face average flux for each face of the cell, i.e.

$$\int_{\partial\Omega} \mathcal{F}_j \cdot d\mathcal{S}_j = \sum_{i=1}^{allfaces} \mathcal{F}_j^i \cdot \mathcal{S}_j^i \tag{2.32}$$

Using this, Eqn. 2.29 becomes

$$\frac{\partial Q}{\partial t} V + \sum_{i=1}^{allfaces} \mathcal{F}_j^i \cdot \mathcal{S}_j^i = 0 \tag{2.33}$$

This equation is then solved iteratively for each cell volume in the computational domain. The time derivatives are solved using a three-stage Runge-Kutta technique. The convective and diffusive fluxes are solved using a low-dissipation third-order upwind-biased scheme and a second-order central difference scheme, respectively. Further information on the numerical scheme and boundary conditions is given in Andersson [45] and Eriksson [47, 50].

Chapter 3

Research objectives

The primary objective of the work done in this thesis is to investigate noise reduction methods for supersonic jets. This is of great importance if supersonic transport is to be reallowed in the future, since the jet is one of the main noise sources of supersonic aircraft along with the sonic boom. Increased aircraft speed results in a drastic increase of the acoustic power because it scales with $I \propto u_{\mathrm{j}}^3$ and therefore underscores the importance of jet noise research and noise control. The objectives of this research evolved as the work progressed and are summarized as follows:

- Predict the flow-field and the noise radiation of a supersonic jet using LES and validate with experimental results from the University of Cincinnati.
- Control the noise radiation from a supersonic jet using fluidic injection.
- Apply various types of fluidic injection; steady, pulsed and flapping.
- Complement experimental data with LES for further insights into the underlying flow physics responsible for noise reduction.
- Analyze the effect of fluidic injection on the jet thrust.
- Investigate the effect of the nozzle inner shape on the jet-flow and the radiated noise.
- Investigate temperature effects on the jet-flow and the radiated noise.

The main achievements of the work are the numerical and experimental evaluation of the flow-field and acoustics of the optimized nozzle design that resulted in improved performance without an acoustic penalty for a wide range of operation conditions. Furthermore, the various fluidic injection configurations that were investigated add to the bulk of knowledge found in the literature on flow control for supersonic jet noise reduction.

Chapter 4

Summary of papers

This chapter gives a summary of the work and results reported in the papers on which this thesis is based.

4.1 Paper I

"Active Suppression of Supersonic Jet Noise Using Pulsating Micro-Jets"

4.1.1 Motivation and Background

Paper I is a direct continuation of the steady injection simulations conducted by M. Burak and published by Perrino *et al.* [51] and Munday *et al.* [52]. Their work focused on investigating a sharp throat supersonic converging diverging nozzle, using trailing-edge fluidic micro-jet injection for noise reduction. The nozzle pressure ratio was kept constant at a slightly over-expanded condition ($NPR = 4.0$) and the injection mass flow rate was varied. The measurements indicated that there is an optimal injection mass flow rate in terms of noise reduction. Furthermore, the measurements showed that the noise reduction for the upstream and the downstream far-field observers was to some extent counterbalanced, i.e. with increased mass flow rate, the measurements showed a decreased $OASPL$ for the upstream observers but an increased $OASPL$ for the downstream observers. Cuppoletti *et al.* [53] investigated the effects of fluid injection, with the same micro-jet set-up at various nozzle pressure ratios and different injection mass flow ratios and made comparisons with an equivalent chevron nozzle. The idea of using injection with pulsating micro-jets has been brought up, since the hope is that it can be more effective than steady-state injection. The work presented by e.g. Samimy *et al.* [54, 55] is an example of successful noise reduction using pulsed injection. They studied the effect of pulsating micro-jets using plasma actuators in high speed jets (Mach 0.9) and achieved a noise reduction of over 1.0 dB for a large range of excitation Strouhal numbers.

4.1.2 Work and Results

The effect of pulsed micro-jet injection on the flow-field and acoustics of a supersonic CD-nozzle at $NPR = 4.0$ was investigated numerically. Two types of pulsation characteristics were tested, i.e. a full and a half sinusoidal injection mass flow rate, using four injection frequencies and two amplitude modulations. The pulsed cases were compared with the flow-field and the far-field acoustics of the baseline nozzle and the fluidic nozzle both with and without steady-state injection. The flow-field and the acoustics of the baseline nozzle and the fluidic nozzle, both with and without steady-state injection, were compared with experimental results. The location of the shocks of the baseline nozzle from the simulations compared well with the experiments. However, the simulations predict a thinner shear layer of the jet at the nozzle exit and a higher spreading rate of the jet compared with the experiments. The simulated noise from the jet agreed with the experimental results within 2.0 dB.

The simulations showed a sensitivity of the radiated noise from the jet to the injection frequency and to the injection type. The half sinusoidal injection introduced tonal noise with a frequency equal to the injection frequency. The pulsed injection also introduced higher harmonics of the injection frequency. Furthermore, the increased injection frequency increased the amplitude of the excited tonal noise and higher harmonics. However, the amplitude of the tonal noise and the subsequent harmonics were decreased by using a full sinusoidal injection.

The half sinusoidal injection performed worse in terms of $OASPL$ compared to the steady-state injection, whereas a noise reduction equal to the steady-state injection was achieved with the full sinusoidal injection. However, there is still a penalty of increased noise for the downstream observers. Since the net mass flow of the pulsed case is less compared to the steady-state injection case, the bleed mass flow from the compressor is lower and hence the impact on the engine efficiency is lower.

4.1.3 Comments

The full sinusoidal injection case at $f_i = 1$ kHz was more effective in noise reduction compared to the corresponding half sinusoidal injection case. However, at the time the paper was written, it was unknown whether this was also the case for higher injection frequencies. This type of comparison was carried out with an injection frequency of $f_i = 7$ kHz, and it turned out that the intensity of the harmonics is lower for the full sinusoidal case, as shown in Fig. 4.1. Furthermore, the $OASPL$ for the observers in the range $\phi \in [80° - 110°]$ is lower compared to the steady-state injection case. This is interesting, since none of the other injection frequencies that were investigated achieved improved noise reduction compared to the steady injection case.

Another interesting observation that was made is that the induced tonal noise is not at equal frequency, although the injection frequency is the same for both of the injection types. In the case of half sinusoidal injection, a tone appears at a frequency (7.4 kHz) higher than the injection frequency, whereas, in the case of full sinusoidal injection, the tone appears at lower frequency (6.7 kHz). This is not fully understood and needs further investigation.

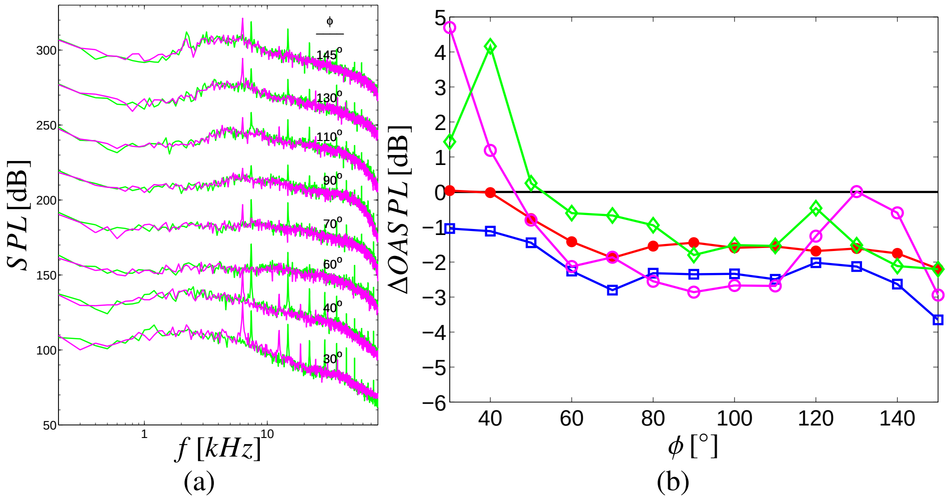

Figure 4.1: (a) SPL versus frequency for different observers. (b) Difference in OASPL compared to the baseline nozzle versus observer angle. Red • No injection, blue □ Steady-state injection, green ◇ Half sinusoidal injection $f_i = 7$ kHz and magenta ○ Full sinusoidal injection $f_i = 7$ kHz.

The highest injection frequency that was tested, in addition to the ones presented in the paper, was $f_i = 40$ kHz and is about the highest frequency which is well resolved using the current computational grid. However, this case did not show any improvement over the steady injection case, as shown in Fig. 4.2.

The numerical study of the pulsed injection was followed up with a joint experimental and numerical study published by Cuppoletti *et al.* [56]. The effect of pulse frequency, duty cycle and injection angle on the noise components for the current jet case was investigated. A previous numerical study had shown that design changes of the experimental pulsed nozzle were needed. The plenum inside the micro-jet channels upstream of the micro-jets exhaust was originally designed to provide equal pressure distribution for the injectors. However, it turned out that it also reduced the amplitude of the pressure pulses and therefore reduced the effectiveness of the pulsed micro-jets. The issue was solved by placing the actuator valves as close as possible to the micro-jet exhaust.

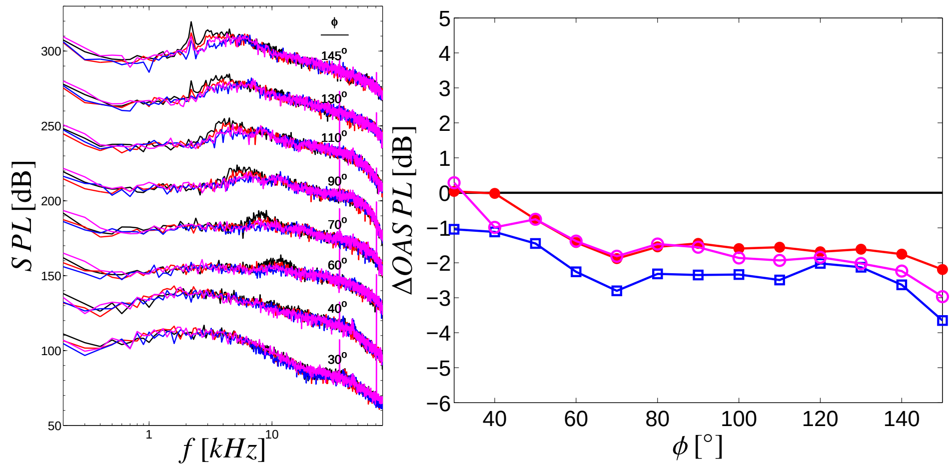

(a) (b)

Figure 4.2: (a) SPL versus frequency plotted against observer angle. (b) Difference in OASPL compared to the baseline nozzle versus observer angle. Black is the baseline, red • No injection, blue □ Steady-state injection magenta ○ Full sinusoidal injection f_i = 40 kHz.

Injection frequencies in the range of $f_\mathrm{i} \in [1 - 400]$ Hz and duty cycles between 20% and 80% were studied. It was clearly demonstrated, with the experimental data, that the noise reduction increased with increased duty cycle, and it was shown that the noise reduction could be scaled based on the duty cycle of the injection pulses, as shown in Fig. 4.3.

In the presented simulations, a pulsed injection with frequencies of $f_\mathrm{i} = 10$ Hz, $f_\mathrm{i} = 50$ Hz and $f_\mathrm{i} = 100$ Hz is applied. These frequencies are relatively low in comparison with the timescales involved in the jet and therefore act to some extent as a quasi-steady state injection. A low pulsed injection frequency is a challenge from a numerical simulation point of view compared to higher pulsation frequencies, since a longer sampling time is needed if an equal amount of pulsed periods are to be sampled. Due to the quasi-steady state behavior, the computational time can be decreased by sampling over a fewer number of injection periods without a critical sacrifice of accuracy. However, it must be kept in mind that the sampling length is restricted to a complete number of injection periods. One injection period might be sufficient to get a rough first estimate of the flow and acoustic statistics for the lowest injection frequency ($f_\mathrm{i} = 10$ Hz). The LES/CAA predicts a minimal difference for the three frequencies that were simulated, which is in agreement with the overall trend observed in the experiments, as shown in Fig. 4.4.

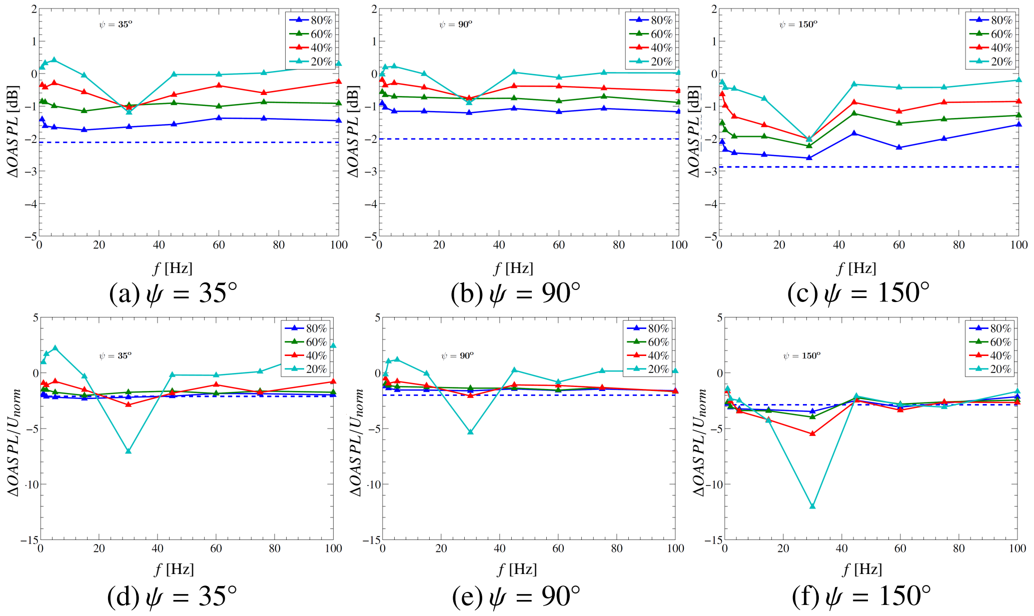

(a) ψ = 35° (b) ψ = 90° (c) ψ = 150°

(d) ψ = 35° (e) ψ = 90° (f) ψ = 150°

Figure 4.3: Experimental results showing the effect of duty cycle on the noise radiation compared to the baseline case. The dotted line corresponds to the noise reduction of the steady injection case. Adapted from [56].

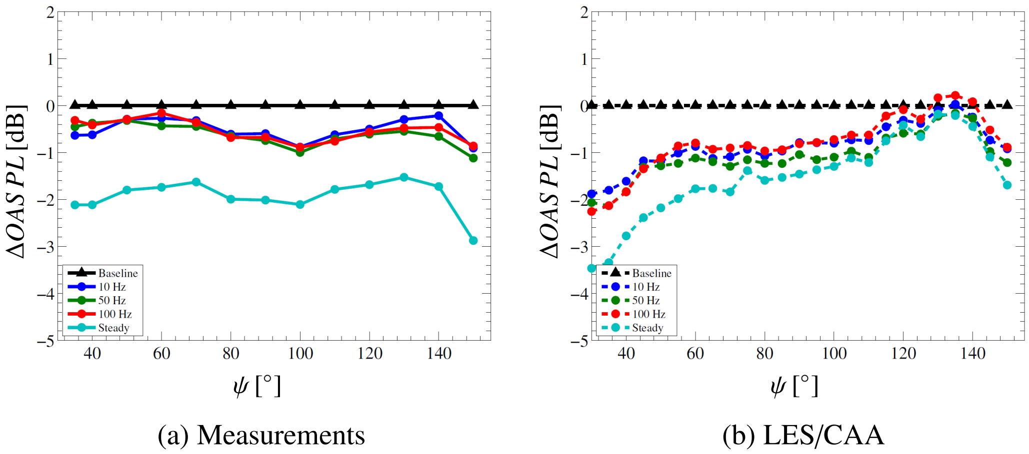

(a) Measurements (b) LES/CAA

Figure 4.4: Comparison of the effect of low frequency pulsed injection on noise reduction of the baseline case. Adapted from [56].

4.2 Paper II

"Noise Control of Supersonic Jet with Steady and Flapping Fluidic Injection"

4.2.1 Motivation and Background

The induced pressure peaks caused by the pulsed injection led us to investigate other transient fluidic methods in the hope for reduced tonal noise. The goal of this study was to implement a boundary condition that could represent a flapping fluidic actuator and then apply the actuation to the supersonic jet.

4.2.2 Work and Results

In this study, the injector cross-sectional area, the number of injectors and the injection mass flow were varied. These modifications were shown to have the same effect: increased injection penetration and hence increased streamwise vorticity. Increased streamwise vorticity increases the initial turbulence kinetic energy (TKE) near the nozzle exit and increases jet dissipation, which results in lower TKE further downstream and hence reduced mixing noise. Flapping injection was applied to the different injection configurations. It was shown that the flapping injection did not excite pressure peaks similar to those previously observed in the case of pulsed injection. However, the far-field noise reduction of the investigated flapping injection cases did not improve the noise reduction compared to the steady injection cases. The case with the largest injection penetration and highest flapping angle amplitude was different compared to the other flapping cases. Strong tonal noise and higher harmonics were detected for all observer angles in the far-field. These tones were found to be created as a combination of two different jet mechanisms. First, at high injection amplitude, the injectors periodically eject out of the shear layer, creating turbulent structures that are convected downstream by the mean flow and radiate noise through shock interaction. Second, the periodic injection directed towards the jet center axis results in a harmonic motion of the shock attached to the nozzle exit and the shock originating from the nozzle throat. The axial distance between the two shock structures changes periodically and causes constructive superposition of the shocks and a tone noise is radiated to the far-field as a result.

4.2.3 Comments

The results indicate that there is no additional noise reduction with flapping injectors. This is positive, since steady injection is expected to be easier to implement for full-scale jet engine applications. However, the parameter space is large and further investigation might reveal potential benefits of the flapping injection.

4.3 Paper III

"LES study of Screech Mechanism and the effect of Micro-Jet Injection"

4.3.1 Motivation and Background

Screech in supersonic jets has been studied extensively ever since it was first reported by Powell in 1953 [57]. The screech is thought to arise due to a feedback mechanism. Turbulent instabilities in the shear layer that originate at the nozzle exit, propagate downstream, grow in magnitude and start interacting with the shock structure and trigger acoustic radiation that propagates mainly upstream. Those acoustic waves excite turbulent instabilities upon reaching the nozzle lip, and the feedback loop is thereby closed. The frequency of the screech is found to decrease with increased jet Mach number. Screech has also been shown to exhibit different types of modes depending on the jet Mach number. Those modes are found to be axisymmetric, helical or flapping, where flapping modes are a combination of two helical modes rotating in opposite directions.

4.3.2 Work and Results

The screech mechanism of a supersonic jet emitted from a bi-conical nozzle with a sharp throat operated at $NPR = 4.0$ was investigated with LES, and the effect of activated trailing edge injection was studied. The flow was sampled along the jet axis at two radial locations and eight azimuthal locations. The two radial locations were inside and outside the supersonic jet core, respectively. The spectra, auto-correlation and cross-correlations were computed from the time traces.

Spectral analysis of the pressure signal showed that a distinct tone exists, at both radial locations, matching the frequency of the far-field screech. Activated injection reduced the intensity of the tone at both radial locations. The onset of the tone at the inner radial locations was delayed, whereas it was barely noticeable at the outer radial location. Furthermore, spectral intensity aligns with the shock structure and peaks at equal axial intervals as the peak pressure.

The auto-correlations showed strongest the coherence in an axial span of $x/D \approx 4-8$ for the case with deactivated injection, whereas it shifts downstream to $x/D \approx 7-10$ for the case with activated injection and is reduced to a large extent. The time lag between the peaks of maximum correlation matches the time period of the screech tone. Furthermore, the shock structure interrupts coherence at the axial location of peak pressure.

Cross-correlations were used to identify the motion of the pressure and the velocity disturbances. The pressure correlations indicated harmonic upstream propagation at both radial locations, and the velocity correlations showed downstream propagation of turbulent structures. These findings indicate that the downstream propagating turbulent structures excite acoustic waves that propagate upstream, in accordance with the theory proposed by Powell [57]. However, upstream propagation of any structure within the supersonic jet is not possible. In the case of a helical acoustic propagation, although the group velocity is always limited to the speed of sound, the phase velocity of the wave can be supersonic, and that is what is identified in the cross-correlation plots. Furthermore, cross-correlations in the tangential direction confirmed helical propagation of the pressure waves. Activated injection highly reduced the coherence of the pressure fluctuations, whereas small difference in velocity cross-correlations was observed, indicating small changes in convective velocity. Interestingly, although the helical mode is disrupted at the outer radial locations in the subsonic region, the jet still exhibits a weaker helical mode within the supersonic jet core.

The work presented in the paper is the first time, to the author's knowledge, that the screech tone is identified in the supersonic region of the jet and where upstream propagation of an acoustic wave is found inside the supersonic free stream jet.

4.3.3 Comments

A further study on the screech mechanism has been conducted by Larusson *et al.* [58] using a method based on the Arnoldi algorithm [59] and Dynamic mode decomposition (DMD) [60] respectively. Three modes were identified with the Arnoldi method, as possible candidates for the screech mechanism: two helical ($m = 1$) and one axisymmetric ($m = 0$). The frequencies of the helical modes were slightly lower compared to the screech frequency obtained with the LES. This was expected since the shock cell spacing of the baseline flow for the Arnoldi method was marginally larger compared to the LES. The frequency and damping coefficient of the least damped modes from the Arnoldi method, that had a frequency near the screech frequency, are shown in Tab. 4.1, and a visual representation of the modes is shown in Figs. 4.5-4.6. Animations of the evolution of the modes revealed a feedback loop mechanism, similar to what is generally thought to contribute to the screech tone. It was clear from both the helical and the axisymmetric modes that an acoustic wave was traveling upstream outside the jet. Interestingly, a wave was found to be traveling upstream in the supersonic jet core in accordance with the observations found from the cross-correlation plots.

The DMD from a series of consecutive snapshots from the LES, for this particular nozzle condition, did not show any clear evidence of helical modes linked to the screech mode. The coherent motion of the screech was thought to be covered by the turbulent motion of the supersonic jet. An alternative approach was therefore chosen. The flow was perturbed using a continuous circumferential injection at the nozzle trailing edge. The injection was turned on until the shock structure reached quasi-equilibrium; thereafter the injection was turned off and the pressure field was sampled until the shock structure reached the original position. This process was repeated, and a phase average of the sampled time series

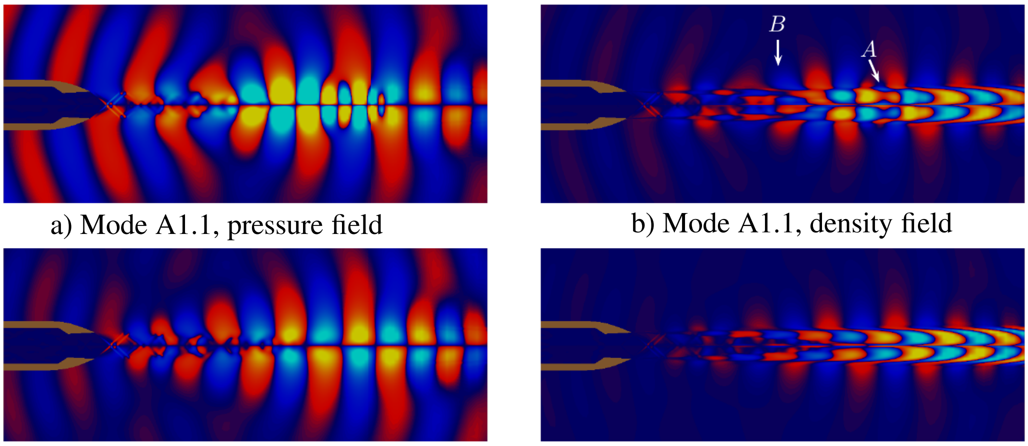

a) Mode A1.1, pressure field

b) Mode A1.1, density field

c) Mode A1.2, pressure field

d) Mode A1.2, density field

Figure 4.5: Helical modes ($m = 1$) from the Arnoldi method. The corresponding frequency and damping coefficient are listed in Tab. 4.1. Adapted from [58].

was obtained and the stochastic fluctuation of the flow was reduced. Nevertheless, no helical motion of the jet was captured with the DMD. Although hard to prove, the absence of helical motion is thought to be related to the time lag for the screech mechanism to develop after the injection is turned off. Cuppoletti *et al.* [56] estimated the shock structure to stabilize in approximately $t = 1.4$ ms, whereas the screech did not fully develop until $t = 5$ ms. For the LES case, a pulsed injection frequency of $f_i = 100$ Hz and a duty cycle of 50% was applied, which gives a total time of $t = 5$ ms where the injection is deactivated and the flow is sampled. Therefore, the screech probably does not pick up its strength within the time frame during which the injection is deactivated. If this is the case, the time laps between activated injection need to be increased to capture screech with the DMD. The least damped modes, from the DMD of the LES, that had a frequency near the screech tone are shown in Fig. 4.7. It can be speculated that a slight helicity appears in the downstream part of the potential core for the L2 mode.

As a final note, DMD was recently carried out at $NPR = 3.5$. The jet exhibits stronger helical screech for that nozzle condition. It turns out that, for this case, the DMD clearly captures the helical mode.

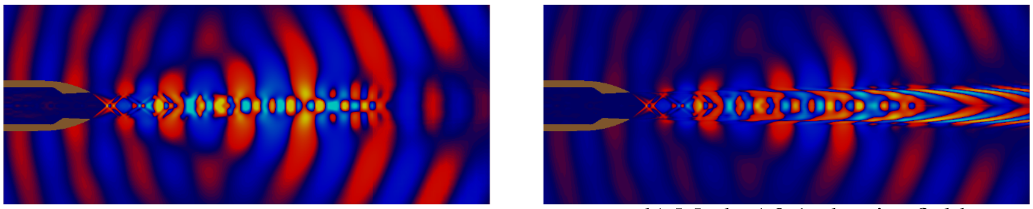

a) Mode A0.1, pressure field

b) Mode A0.1, density field

Figure 4.6: Symmetric modes ($m = 0$) from the Arnoldi method. The corresponding frequency and damping coefficient are listed in Tab. 4.1. Adapted from [58].

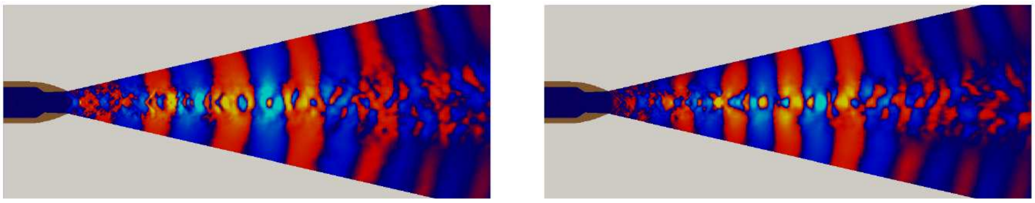

a) L1

b) L2

Figure 4.7: DMD modes from LES. The corresponding frequency and damping coefficient are listed in Tab. 4.1. Reproduced from [58].

Table 4.1: Frequency, f, and damping factor, ξ, for selected Arnoldi modes (A) and DMD LES modes (L). Reproduced from [58].

mode	m	f **[Hz]**	ξ **[s^{-1}]**
A1.1	1	1968	-46
A1.2	1	2195	-502
A0.1	0	2557	-542
L1	-	1858	-2310
L2	-	2395	-1736

4.4 Paper IV

"The Response of Supersonic Jet Noise Components to Fluidic Injection Parameters"

4.4.1 Motivation and Background

The purpose of the work published in the paper was to identify the response of the flow and the acoustics to injector angle, momentum flux ratio and the number of injectors.

4.4.2 Work and Results

This study investigated the effect of injection angle (θ_i), momentum flux ratio (J) and number of injectors on the flow field and acoustics of a supersonic jet. Injector angles of $\theta_\mathrm{i} \in [30°, 45°, 60°, 90°]$ were studied, and the momentum flux ratio was varied between $J = 0.71$ and $J = 1.35$ for a $M_\mathrm{j} = 1.56$ jet. The number of injectors was altered between 6 and 12 and they were equally distributed around the nozzle exit in both cases.

The injection penetration towards the jet axis was shown to be an important parameter for a reduction of mixing noise. The maximum reduction was achieved with the highest injection angle and injection momentum ratio for both the 6 and the 12 injector cases, whereas a minimum shock noise was observed, depending on the injection configuration, as a consequence of breakdown of the shock strength. The 6 injector configuration turned out to be more efficient in terms of mixing noise reduction.

4.4.3 Comments

A hypothesis was proposed for a relation between mixing noise reduction and axial vorticity growth. Fewer injectors allow increased space for the growth of vorticity that resulted in reduced downstream turbulence and hence reduced mixing noise. The 12 injector case showed that the vorticity dissipated further upstream compared to the case with 6 injectors, because of neighboring vortex interaction. However, further analysis is needed to fully support the proposed hypothesis.

4.5 Paper V

"Analysis of Supersonic Jet Thrust with Fluidic Injection"

4.5.1 Motivation and Background

Supersonic jet noise reduction with fluidic injection is closely tied to the thrust criteria. Mixing noise devices, such as chevrons, tabs and fluidic injectors, tend to reduce thrust with reduced noise emissions. The purpose of this study was to investigate the effect of fluidic injection on thrust.

4.5.2 Work and Results

The LES data from the fluidic injection cases presented in paper IV were used to analyze the effect on thrust. The nozzle was operated at design condition, the injection angle was 60° in relation to the flow axis and the difference between 6 and 12 active injectors was studied. A surface integral approach was used to compute momentum and pressure thrust. However, in the experiment, it is difficult to obtain a proper surface integral estimate of a non-axisymmetric exit plane, such as in the case of fluidic injection. Therefore, pressure and momentum thrust from LES for the axisymmetric baseline nozzle, at over-expanded, design and under-expanded jet conditions, were validated with measurements. The surface integrals were shown to match well, except for the highly over-expanded jet where LES predicted a premature separation. Previous comparisons of the axial flow and far-field acoustics showed good match between experiments and LES for the injection cases studied and provided confidence in accurate prediction of the flow with the LES. Hence, the LES was employed as a database for thrust computations. Interestingly, the fluidic injection resulted in reduced momentum thrust with increased injection mass flow, whereas increased pressure thrust was observed due to changes in shock structure at the nozzle exit. The total thrust increased, whereas the specific thrust was reduced with increased injection mass flow, and 6 injectors were shown to perform better than 12 injectors.

4.5.3 Comments

Full system performance analysis is needed to fully quantify the effect of fluidic injection on the thrust. Injection air, bled from the high or low pressure compressor, might reduce the efficiency of the engine. However, it is interesting to point out that, although the specific thrust goes down, the injection increases thrust. Furthermore, the injection will only be operated during critical conditions, such as take-off, while it will be turned off the rest of the flight time and hence the engine performance will be unaffected.

4.6 Paper VI

"The role of Nozzle Contour on Supersonic Jet Thrust and Acoustics"

4.6.1 Motivation and Background

The sharp throat inside the nozzle causes the creation of a shock by the impinging flow. The shock propagates downstream with the flow and is reflected by the nozzle geometry and the jet shear layer. Furthermore, if the nozzle exit is not perfectly expanded, an additional shock will be created at the nozzle lip which also propagates downstream inside the jet plume as it reflects on the jet shear layer. Those two shocks will create a double diamond shock structure inside the jet plume which gives rise to a shock associated noise. It was investigated in this paper whether a reduction of the inner shock would result in a lower radiated noise.

4.6.2 Work and Results

The angle of the converging part of the nozzle and the throat corner radius were varied. The effect of the two variables on the performance of the nozzle was investigated by Dr. Bernhard Gustafsson at GKN Aerospace in Trollhättan, Sweden. A design of experiments with 12 designs and a subsequent response surface with 3000 designs was created from the RANS. A design was chosen that minimized the outlet Mach number and the velocity uniformity. This design has a much smoother inner contour than the original design; consequently, the shock created at the throat was nearly eliminated. The optimized geometry was manufactured at the University of Cincinnati, where it was tested experimentally by D. Cuppoletti and further investigated numerically by Dr. Bernhard Gustafsson using RANS and, at Chalmers, using LES. The radial profiles of the turbulence kinetic energy from the SST-k-ω model and the LES compare well near the nozzle exit, while the SSG-RSM and the LES compare better further downstream. The PIV showed trends similar to both the RANS and the LES. However, a better match was obtained with the axial velocity compared to the kinetic energy. The optimized nozzle has an increased thrust of 3.9 % and a mass flow of 4.5 % compared to the sharp throat nozzle at NPR=4.0.

4.6.3 Comments

At fully expanded conditions, the radiated noise from the sharp nozzle (NPR=4.5) and the optimized nozzle (NPR=4.27) is almost identical for all observers. The main benefit of the optimized nozzle is that thrust equal to the sharp nozzle is obtained with a lower pressure ratio without an acoustic penalty.

4.7 Paper VII

"Exploration of temperature effects on the far-field acoustics radiation from a supersonic jet"

4.7.1 Motivation and Background

The capability of the compressible flow solver to capture the flow dynamics and the far-field acoustics of a heated jet were investigated. The work presented in the paper is a step toward simulating jet temperatures encountered in real flight operations.

4.7.2 Work and Results

Temperature effects on the flow field and far-field acoustics of a supersonic jet emitted from a biconical nozzle with a sharp throat was investigated using LES and validated with experimental data. The nozzle was operated at slightly underexpanded conditions ($NPR = 4.0$) and at three nozzle temperature ratios of $NTR \in [1, 2, 3]$.

It should be noted that the nozzle is smaller in size compared to the nozzle that was used for all the other simulations in the thesis. The nozzle is smaller because the jet exit temperature in the experiment is limited by the mass flow. Therefore, the work included meshing of the new nozzle geometry. The smallest cell size was reduced as a result of a smaller nozzle, and that put a constraint on the time step for the simulations. Consequently, the spatial resolution of the simulations is increased, and that gives increased high-frequency resolution of the acoustic spectra.

The predicted far-field acoustics were shown to match well with the experimental data. However, the lower part of the frequency range appeared to be underpredicted by the LES/CAA for the high temperature cases ($NTR = 2$, $NTR = 3$). This mismatch is thought to be related to acoustic reflections of the surrounding walls in the experimental rig. Padding was added to the anechoic chamber, and that improved the acoustic spectra within the particular frequency range. Further improvements of the anechoic chamber are thought to bring the predicted and measured acoustic levels even closer. The downstream mixing noise was shown to be in very good agreement, whereas the direction of the peak $OASPL$ was off by around $\Delta\phi \approx 10^\circ$ for the highest jet temperature. This difference is thought to be related to a temperature difference due to heat convection through the nozzle walls and the pipe upstream of the nozzle. However, further investigation is needed to verify that.

Crackle [61] is an annoying sound component that may arise in heated jets. It does not appear in the acoustic spectra, and therefore other measures such as pressure skewness are commonly used for that purpose. It was investigated whether crackle could be captured with an acoustic analogy such as the Kirchhoff surface integral method. The pressure skewness of the far-field pressure signal from the LES/CAA was computed and compared with experimental values. The LES/CAA underpredicts the pressure skewness, but the trends were generally in good agreement.

Pressure data from Pitot tube measurements in the jet core compared very well with the predicted pressure field from the LES. The location and the magnitude of the shocks were both in good agreement. The dominant noise source locations were identified with snapshots of instantaneous data from the LES, and the angle of the dominant acoustic waves was shown to match with the peak propagation angle in the far-field acoustic spectra.

4.7.3 Comments

The mismatch between the predicted and measured far-field pressure skewness implied further investigation of the acoustics near the Kirchhoff surface. The warmest jet configuration ($NTR = 3.0$) was chosen. A series of monitor points were placed along the direction of the peak acoustic propagation ($\phi = 50°$) in a region of high near-field acoustic radiation, as shown in Fig. 4.8. Interestingly, the skewness near the Kirchhoff surface is similar to the predicted far-field skewness. This indicates accurate capture of the skewness by the Kirchhoff integral method. Moreover, it can be noted that the skewness increases with increased propagation distance from the noise source, reaches a maximum and then falls off due to decreased mesh resolution. Increased skewness values might be a result of a wave steepening due to a non-linear propagation, and that could be an explanation of the difference between the predicted and measured far-field pressure skewness.

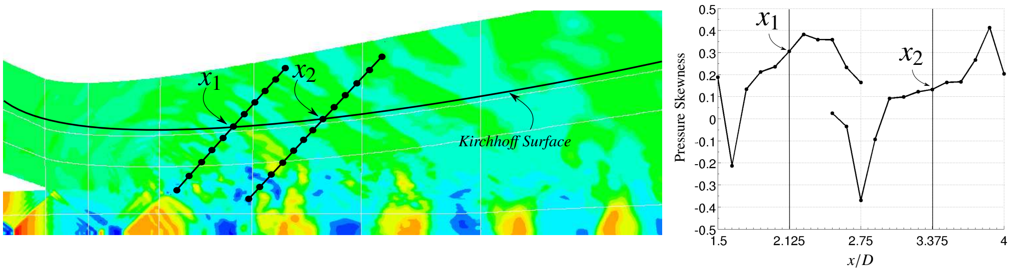

(a) (b)

Figure 4.8: (a) Instantaneous flow field for the case with $NTR = 3$. The two parallel lines show the probe locations. The x_1 and x_2 show the intersection of the probe points with the Kirchhoff surface. (b) Pressure skewness for each probe point.

A constant viscosity at standard sea level condition was specified for all simulations presented in the paper. However, at such high temperatures, the viscosity of air changes significantly, as described by Sutherland's law:

$$\mu = \mu_0 \left(\frac{T}{T_0}\right)^{3/2} \left(\frac{T_0 + S}{T + S}\right) \tag{4.1}$$

Here, T_0 is a reference temperature, μ_0 is viscosity at the reference temperature and S is the Sutherland's temperature. The reference values for air are given in Tab. 4.2.

Table 4.2: Sutherland's law reference values

μ_0[kg/ms]	T_0[K]	S[K]
1.716×10^{-5}	273.15	110.4

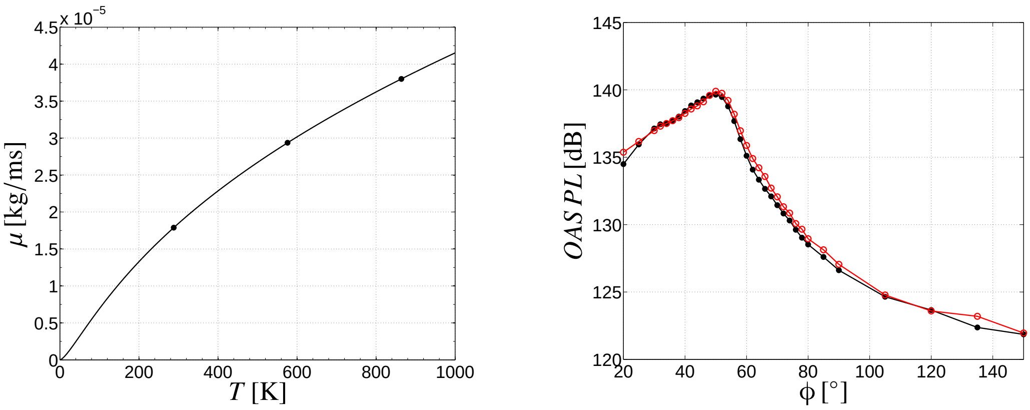

(a) (b)

Figure 4.9: (a) Viscosity of air vs. temperature. Bullets (•) mark the jet temperature configurations presented in the paper, $NTR \in [1, 2, 3]$. (b) Far-field $OASPL$ vs observer angle ϕ. Black (•): Constant viscosity, Red (○): Corrected viscosity.

The viscosity is roughly doubled with increased temperature from $NTR = 1$ to $NTR = 3$, as shown in Fig. 4.9(a). Nevertheless, the effect on the far-field $OASPL$ is insignificant, as shown in Fig. 4.9(b). The effect on the jet structure is also minimal, as shown in Fig. 4.10-4.11. However, at the end of the potential core, the shocks shift slightly upstream and are moderately weaker. Reduced shock strength at the end of the potential core, where the velocity is lower, is expected, since the viscous dissipation is increased. The pressure change of the first shock is slightly increased with increased viscosity. Furthermore, slightly lower turbulence kinetic energy (TKE) is observed near the nozzle exit for the higher viscosity case, whereas, the TKE increases downstream of the first shock shear layer interaction ($x/D \approx 1$). The increased TKE is thought to be a combination of two effects: first, the increased pressure of the first shock triggers higher turbulence through shock shear layer interaction and, second, lower initial turbulence levels generally result in increased turbulence downstream, once initiated [62]. However, it should be emphasized that the difference is relatively small, which indicates that the turbulent viscosity is already dominant over the dynamic viscosity. Furthermore, Morris [63] showed by stability analysis of free jets that viscous effects are greatly diminished at high Reynolds numbers. Moreover, Liu *et al.* [64] showed that inviscid LES captures the flow fields and the far-field acoustics of imperfectly expanded supersonic jets.

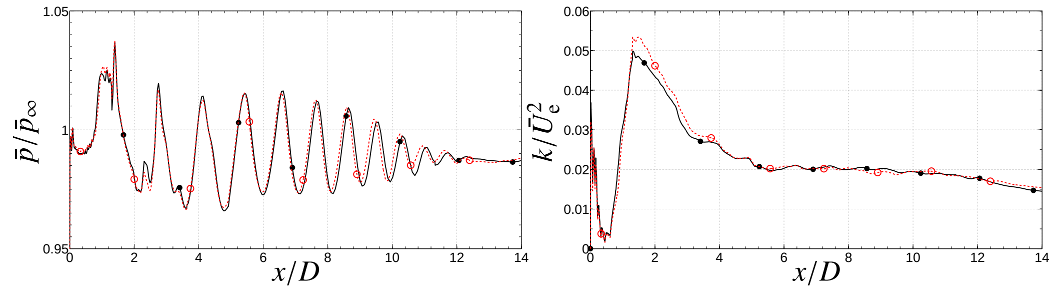

(a) (b)

Figure 4.10: Flow profile at $r/D = 0.5$. Black Cont. (∘): Constant viscosity, Red Dotted (∘): Corrected viscosity.

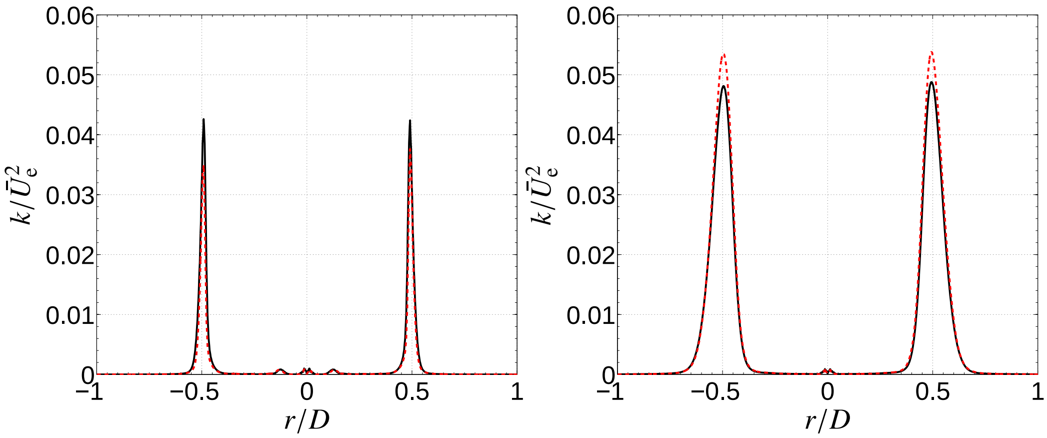

(a) (b)

Figure 4.11: Profiles of turbulence kinetic energy at two axial locations (a) $x/D = 1.0$ (b) $x/D = 1.5$. Black Cont. (•): Constant viscosity, Red Dotted (∘): Corrected viscosity.

Chapter 5

Unpublished Results

5.1 Internal Injection

5.1.1 Motivation and Background

Effective mixing noise and shock noise reduction for the external and trailing edge injection cases invoked an interest in injecting directly to the divergent section of the nozzle, as an attempt to reduce the strength of the shock attached to the nozzle throat. FMV has a patent application pending for the design of the internal injection configuration presented in this section. The joint experimental and computational effort was conducted in 2011.

5.1.2 Work and Results

Twelve evenly distributed injectors in the divergent part of the nozzle, $x/D = 0.22$ downstream of the throat, were applied for flow control. The injection angle was 60° in relation to the flow axis. A grid smoothing routine applied to the mesh surface and interior near injectors ensured a high grid quality, as shown in Fig. 5.1. The nozzle was operated at design condition. Five levels of injection mass flow were specified, and the effect on the jet flow and far-field acoustics was studied. Three of the investigated injection mass flow cases are presented in Tab. 5.1. Increased injection mass flow caused the average exit velocity to decrease, whereas the average exit pressure increased due to a changed nozzle exit shock structure. Consequently, increased injection mass flow caused decreased momentum thrust and increased pressure thrust. Increased injection mass flow caused increased total thrust and decreased specific thrust, based on net nozzle exit mass flow. The maximum specific thrust loss was $\Delta F_s \approx 1.6\,\%$, which is considered a low penalty compared to the gain in overall noise reduction.

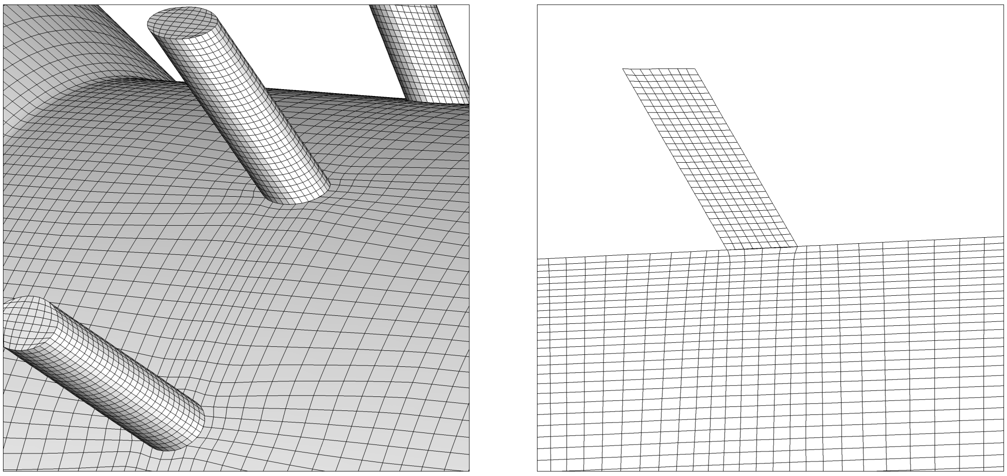

(a) (b)

Figure 5.1: Computational grid near internal injectors

Table 5.1: Effect of net internal injection mass flow $\dot{m}_\mathrm{i}$ on mean nozzle exit conditions; Total mass flow: $\dot{m}_\mathrm{e}$, Velocity: $\bar{u}_\mathrm{e}$, Pressure: p_e, Momentum thrust: $F_\mathrm{m} = \int(\rho_\mathrm{e} u_\mathrm{e}^2)\mathrm{dA}$, Pressure thrust: $F_\mathrm{p} = \int(p_\mathrm{e} - p_\infty)\mathrm{dA}$, Total thrust: $F_\mathrm{tot} = F_\mathrm{m} + F_\mathrm{p}$, Specific thrust: $F_\mathrm{s} = F_\mathrm{tot}/\dot{m}_\mathrm{e}$

$\dot{m}_\mathrm{i}$ [kg/s]	$\dot{m}_\mathrm{e}$ [kg/s]	$\dot{m}_\mathrm{i}/\dot{m}_\mathrm{e}$ [%]	$\bar{u}_\mathrm{e}$ [m/s]	p_e [kPa]	F_m [N]	F_p [N]	F_tot [N]	F_s [Ns/kg]
0.000	1.696	0.0	500.0	90.8	849.3	-27.3	822.1	484.7
0.047	1.740	2.8	480.3	99.8	837.9	-4.1	833.9	479.2
0.069	1.762	4.1	474.8	102.8	838.4	3.8	842.3	478.0
0.090	1.784	5.3	469.0	106.0	838.2	12.1	850.3	476.6

The injection mass flow of $\dot{m}_\mathrm{i}/\dot{m}_\mathrm{e} = 4.1\%$ caused significant shock strength weakening, as shown in Fig. 5.2a), whereas the shock strength was barely affected in the case of other injection mass flows. Consequently, the broadband shock associated noise and screech tone noise were significantly reduced, as shown in Fig. 5.2c,d). In contrast, none of the injection mass flow cases caused any considerable mixing noise reduction, due to an insignificant change of turbulence kinetic energy in the shear layer, as shown in Fig. 5.2b).

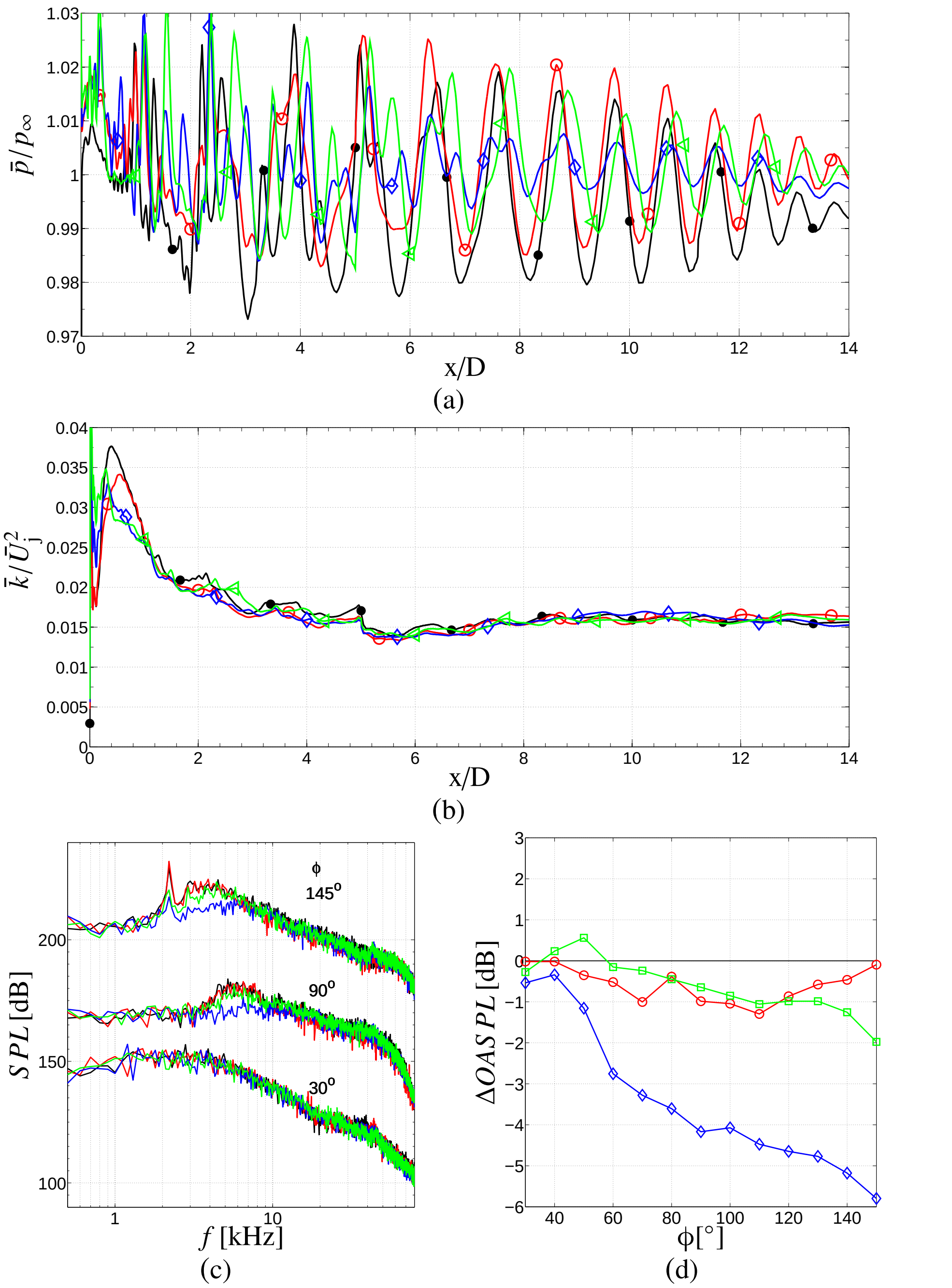

Figure 5.2: (a) Pressure along the $\hat{x}$-axis at radial location of $r/D = 0.5$ (b) Turbulence kinetic energy along $\hat{x}$-axis at radial location of $r/D = 0.5$, (c) Far-field acoustic spectra, (d) Change in *OASPL* compared to the case with deactivated injection. $r/D = 0.5$, • $\dot{m}_i/\dot{m}_e = 0\%$, ○ $\dot{m}_i/\dot{m}_e = 2.8\%$, ◊ $\dot{m}_i/\dot{m}_e = 4.1\%$, ◁ $\dot{m}_i/\dot{m}_e = 5.3\%$.

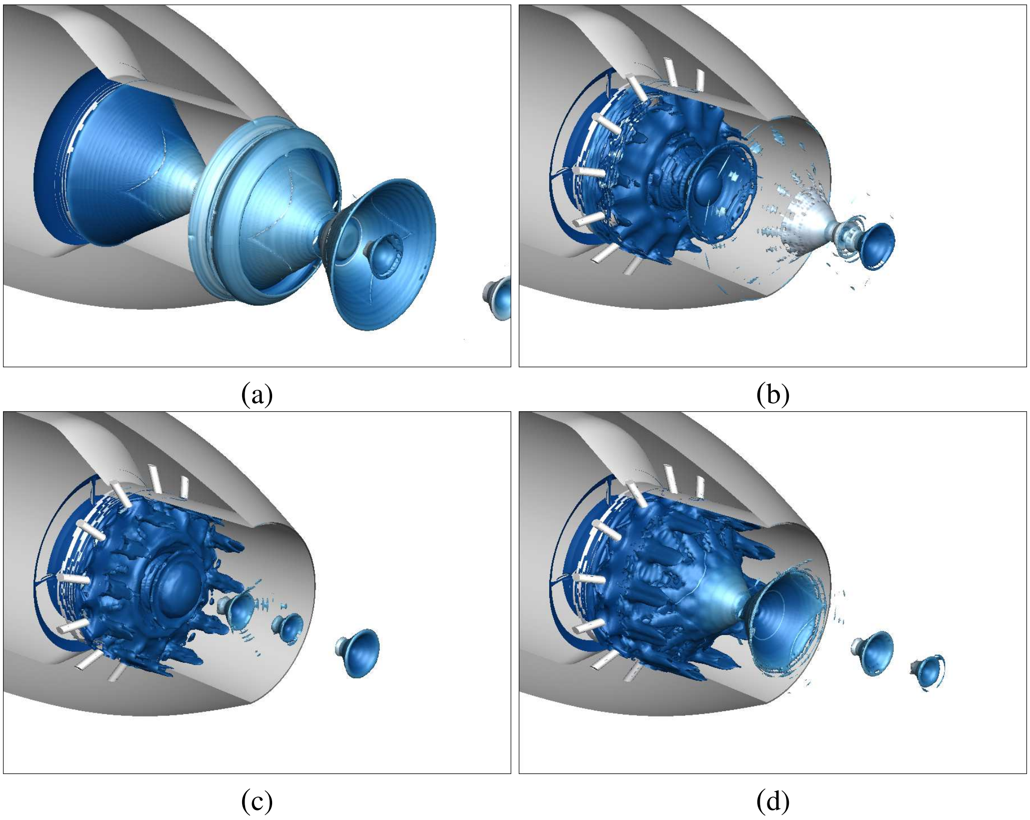

Figure 5.3: Iso-surface of pressure gradient magnitude, (a) $\dot{m}_i/\dot{m}_e = 0\%$, (b) $\dot{m}_i/\dot{m}_e = 2.8\%$, (c) $\dot{m}_i/\dot{m}_e = 4.1\%$, (d) $\dot{m}_i/\dot{m}_e = 5.3\%$.

The fluidic injection forms a complex three dimensional shock-structure in the divergent part of the nozzle through injector/shock interaction (Fig. 5.3). The highly dynamic and turbulent supersonic jet flow is shown in Fig 5.4, and the time averaged flow is shown in Fig 5.5. The internal injection shifts the shock attached to the nozzle throat upstream. The mechanism responsible for reduced jet shock strength, in the optimum injection mass flow case, is an additional shock structure formed at the center of the first shock cell. The extra shock interacts destructively with the original shock-structure, largely reducing the shock strength of the whole supersonic jet.

A wide range of injection pressures was investigated experimentally at two nozzle pressure ratios. When the nozzle was operated at design conditions ($NPR = 4.0$), the broadband shock associated noise was observed to decrease with increased injection pressure, as shown in Fig. 5.6-a). However, a minimum broadband shock associated noise was not fully achieved due to a limitation of the maximum injection pressure. However, when the nozzle was operated at the lower nozzle pressure ratio ($NPR = 2.5$), a minimum of the shock noise was observed, as shown in Fig. 5.6b). The effect of injection pressure on far-field $OASPL$, at three observer angles is quantitatively compared to the corresponding baseline

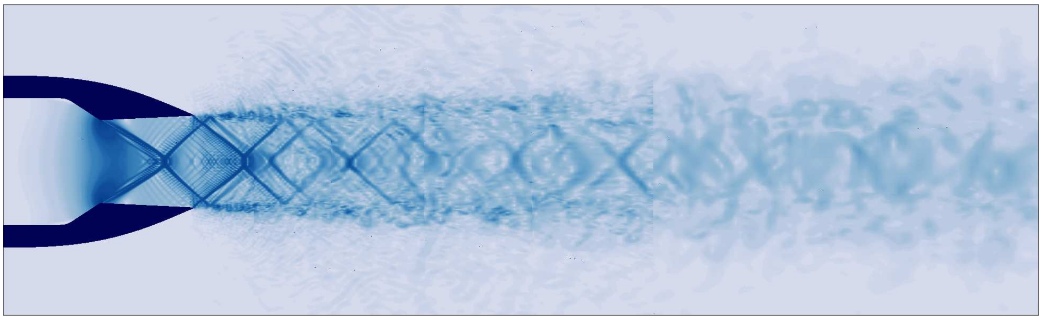

(a)

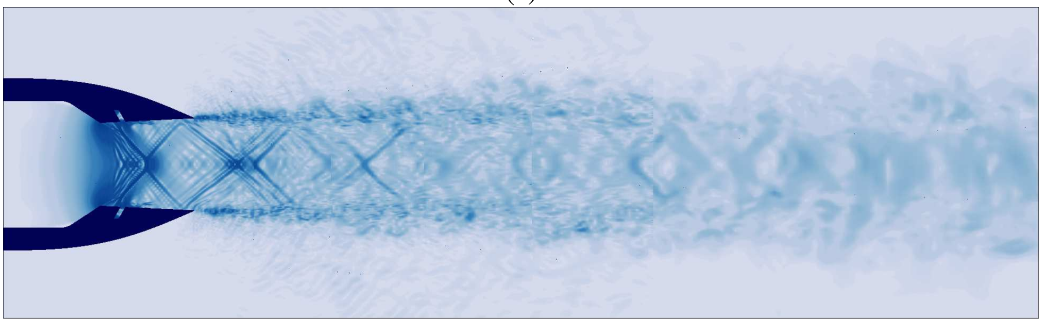

(b)

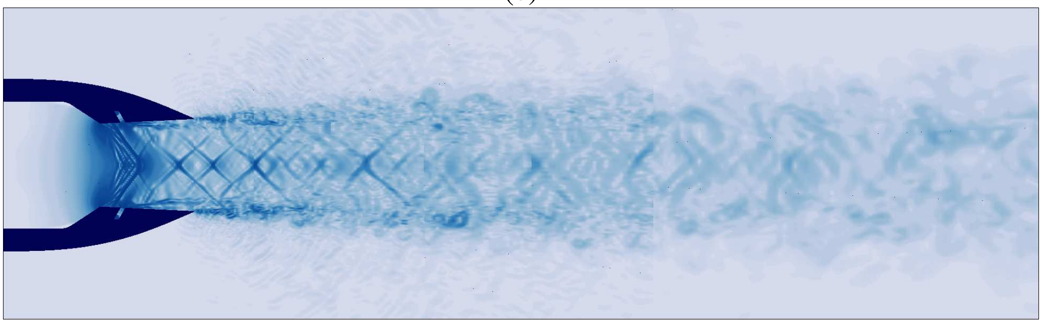

(c)

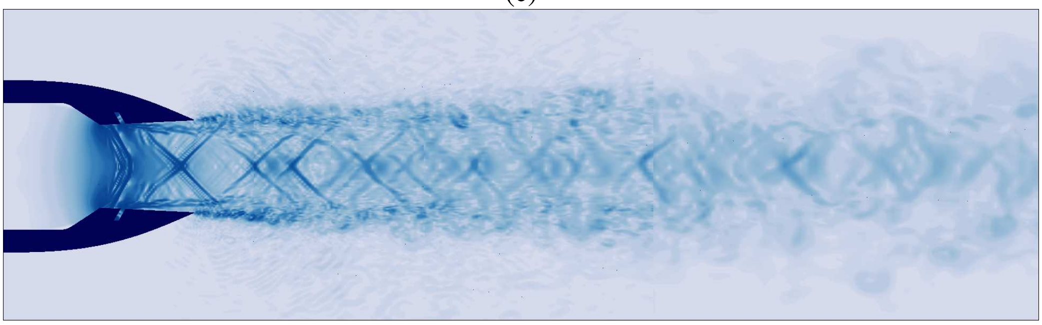

(d)

Figure 5.4: Instantaneous pressure gradient magnitude, (a) $\dot{m}_\mathrm{i}/\dot{m}_\mathrm{e} = 0\%$, (b) $\dot{m}_\mathrm{i}/\dot{m}_\mathrm{e} = 2.8\%$, (c) $\dot{m}_\mathrm{i}/\dot{m}_\mathrm{e} = 4.1\%$, (d) $\dot{m}_\mathrm{i}/\dot{m}_\mathrm{e} = 5.3\%$.

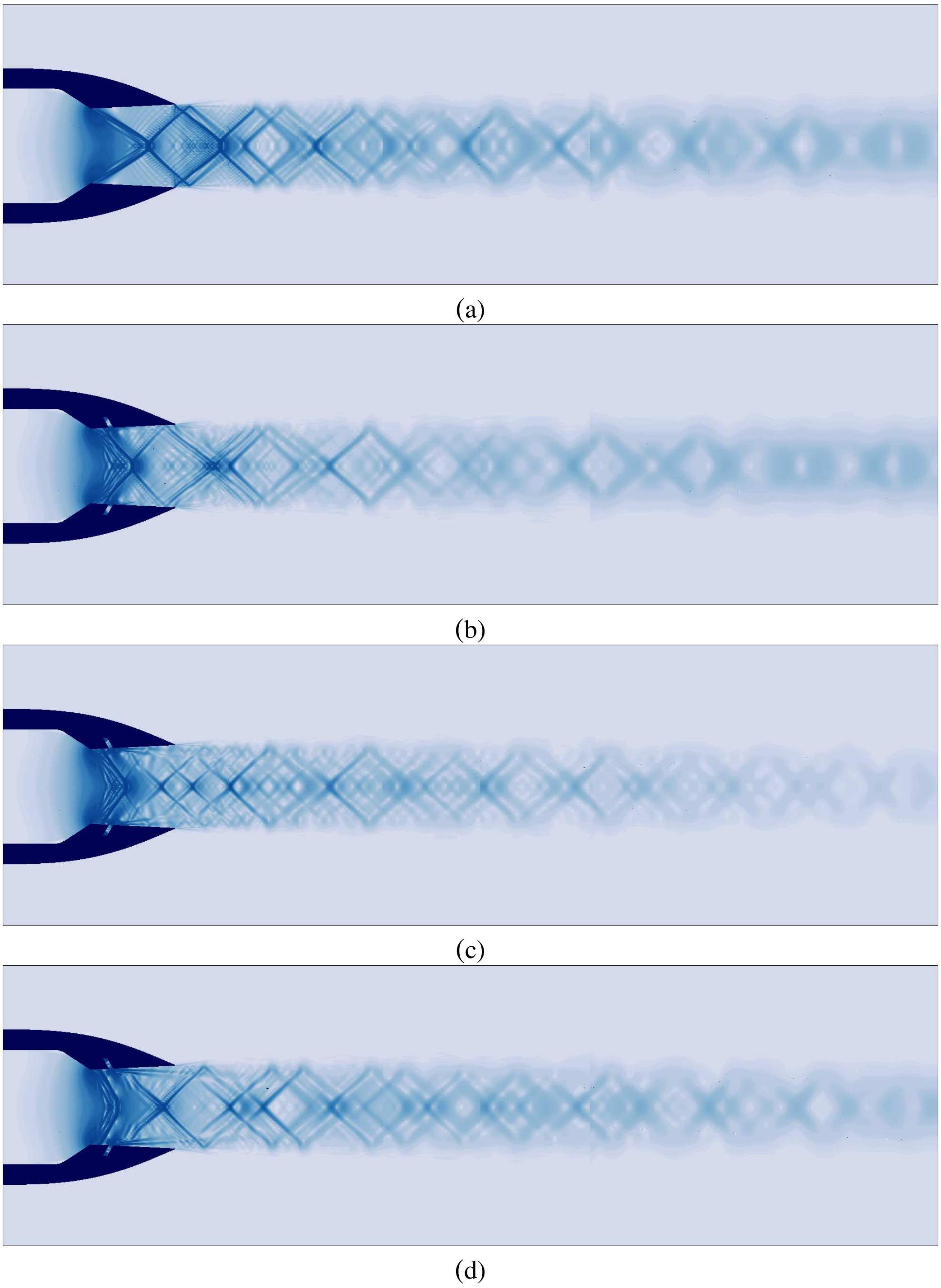

Figure 5.5: Time-averaged pressure gradient magnitude, (a) $\dot{m}_\mathrm{i}/\dot{m}_\mathrm{e} = 0\%$, (b) $\dot{m}_\mathrm{i}/\dot{m}_\mathrm{e} = 2.8\%$, (c) $\dot{m}_\mathrm{i}/\dot{m}_\mathrm{e} = 4.1\%$, (d) $\dot{m}_\mathrm{i}/\dot{m}_\mathrm{e} = 5.3\%$.

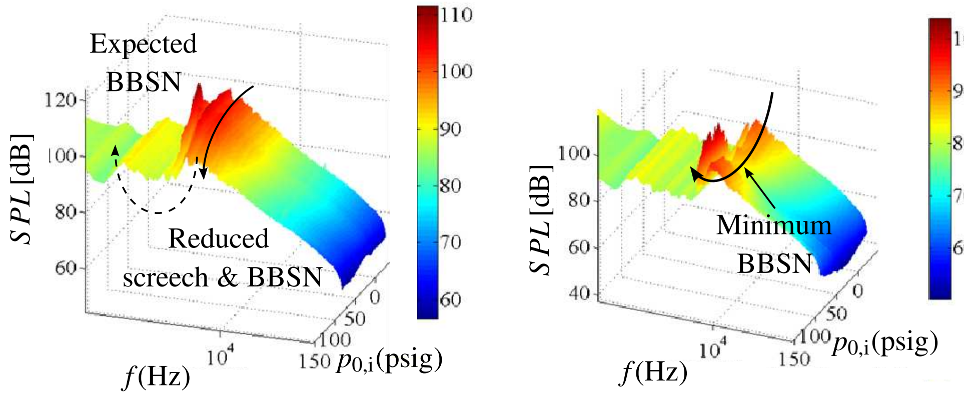

(a) NPR = 4.0, ϕ = 145°

(b) NPR = 2.5, ϕ = 145°

Figure 5.6: Effect of θ_{inj} = 60° injection on acoustic spectra vs. injection pressure for an upstream observer angle of (ψ = 35°). Adapted from [40] with permission.

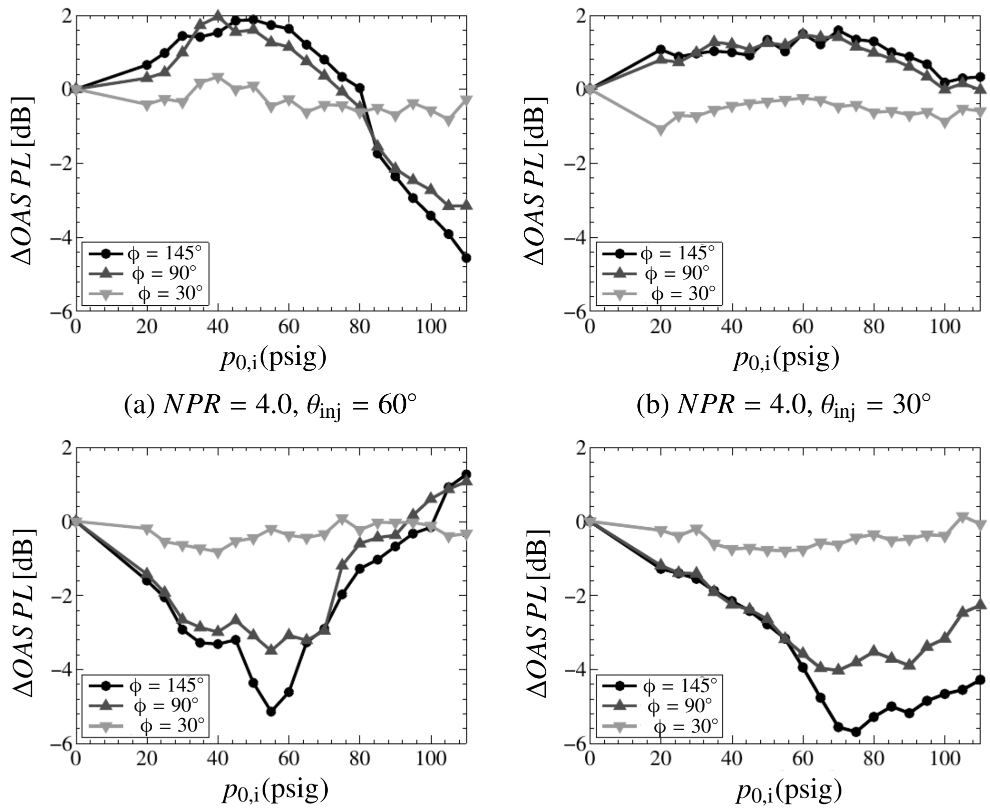

(a) NPR = 4.0, θ_{inj} = 60°

(b) NPR = 4.0, θ_{inj} = 30°

(c) NPR = 2.5, θ_{inj} = 60°

(d) NPR = 2.5, θ_{inj} = 30°

Figure 5.7: Noise levels vs. injection pressure for; upstream (ϕ = 145°), sideline (ϕ = 90°) and downstream (ϕ = 30°) observer angles. Adapted from [40] with permission.

case in Fig. 5.7. Two injection angles are presented ($\theta_{\text{inj}} = 60°$ & $\theta_{\text{inj}} = 30°$). A shallow angle injection ($\theta_{\text{inj}} = 30°$) caused a slight increase in shock noise for most injection pressure ratios, as shown in Fig. 5.7b). A steeper injection angle ($\theta_{\text{inj}} = 60°$) also caused a slight increase in shock noise at low injection pressure, whereas a significant noise reduction was achieved with higher injection pressure, as shown in Fig. 5.7a). The shallow angle injection is more effective for noise reduction at overexpanded condition ($NPR = 2.5$) compared to design condition, where increased injection was observed to decrease shock noise to a minimum point where the shock noise starts to increase with further increase of injection pressure, as shown in Fig. 5.7d). An increased wall normal component of the injection with steeper injection angle causes the optimum shock noise reduction to be achieved at lower injection pressure ratio, as shown in Fig. 5.7c)

A side view zoomed in on a single injector in the divergent part of the nozzle showing Mach number contours reveals the complex injector cross flow interaction, as illustrated in Fig. 5.8. Flow features similar to those presented in section 1.3.2 can clearly be noted. However, additional complexity is introduced by the shock from the nozzle throat that interacts with the micro-jet. The barrel shock and the subsequent Mach disk are formed and the strength increases with increased injection mass flow, as expected. The flow separates upstream of the injector, and a recirculation region is formed that grows larger with increased injection. A small circulation zone can be noted downstream of the injector for the case with the lowest injection mass flow, whereas it does not appear for the other cases. Furthermore, as the mass flow of the micro-jet is increased, a region with a higher Mach number splits up the wake behind the jet along the flow direction.

Mapping of Mach number contours in the $\hat{x}$-plane, at equally distributed axial locations in the divergent part of the nozzle, shows the development of the micro-jet as it convects downstream by the cross flow (Fig. 5.9). The penetration of the micro-jet increases with increased mass flow and increased momentum ratio, as expected. The formation of two counter-rotating vortices can also clearly be noted. The azimuthal spacing between the counter-rotating vortices increases with increased injection mass flow. The azimuthal distance between the two vortices in the vortex pair increases at first as they convect downstream until a point is reached where they appear to approach again and merge, which indicates that an axis switching phenomenon occurs.

5.1.3 Comments

Numerical simulations showed that a steeper injection angle (90°) caused larger upstream shift of the shock attached to the nozzle throat at lower injection pressure, indicating that optimum shock strength breakdown and broadband noise reduction might be achieved with a lower injection mass flow. Moving the injectors closer to the nozzle throat, and hence decreasing the radial distance to the throat shock, is thought to cause a further upstream shift of the shock at even lower

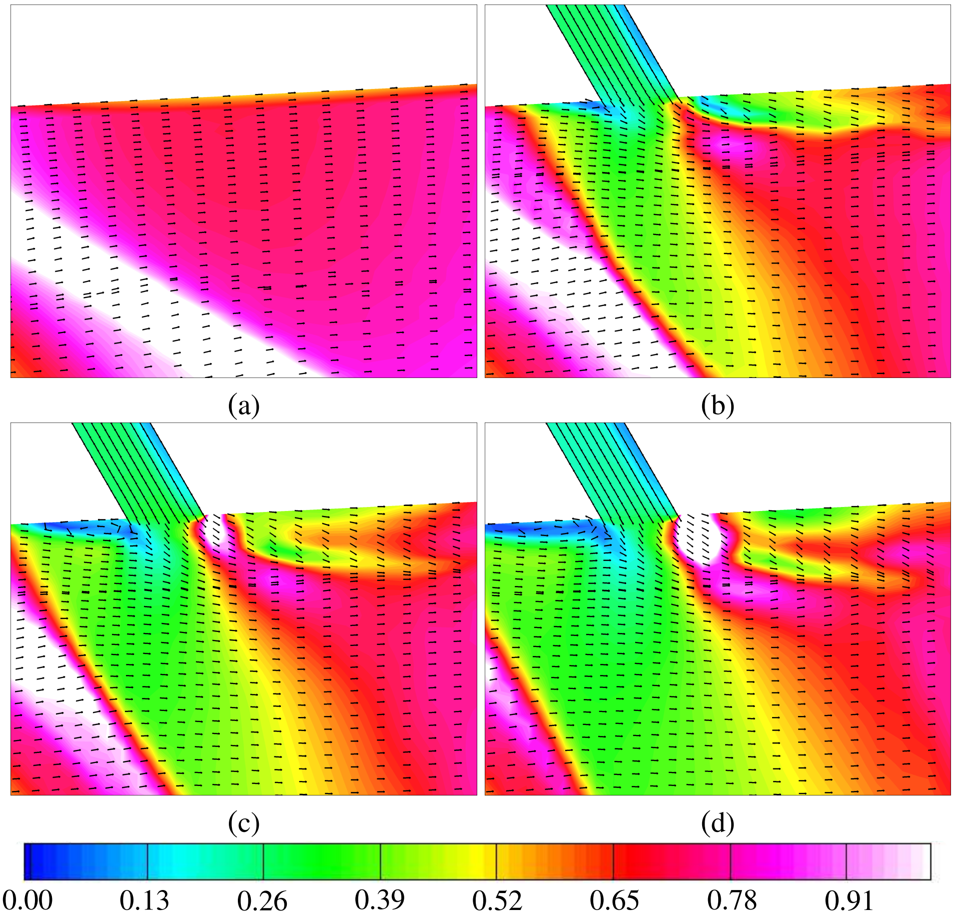

Figure 5.8: Mapping of time-averaged Mach number, viewed from the side of an injector. (a) $\dot{m}_\mathrm{i}/\dot{m}_\mathrm{e} = 0\%$, (b) $\dot{m}_\mathrm{i}/\dot{m}_\mathrm{e} = 2.8\%$, (c) $\dot{m}_\mathrm{i}/\dot{m}_\mathrm{e} = 4.1\%$, (d) $\dot{m}_\mathrm{i}/\dot{m}_\mathrm{e} = 5.3\%$.

injection mass flows. This is however a subject for future research. Potential mixing noise reduction, in addition to the maximum shock noise reduction, could be achieved with a combination of internal and trailing edge injection, since the trailing edge injection showed a large reduction in mixing noise. This is, however, also a subject for future research. Furthermore, 6 injectors instead of 12 are potentially more robust for improved mixing noise reduction, due to the greater room for axial vorticity growth.

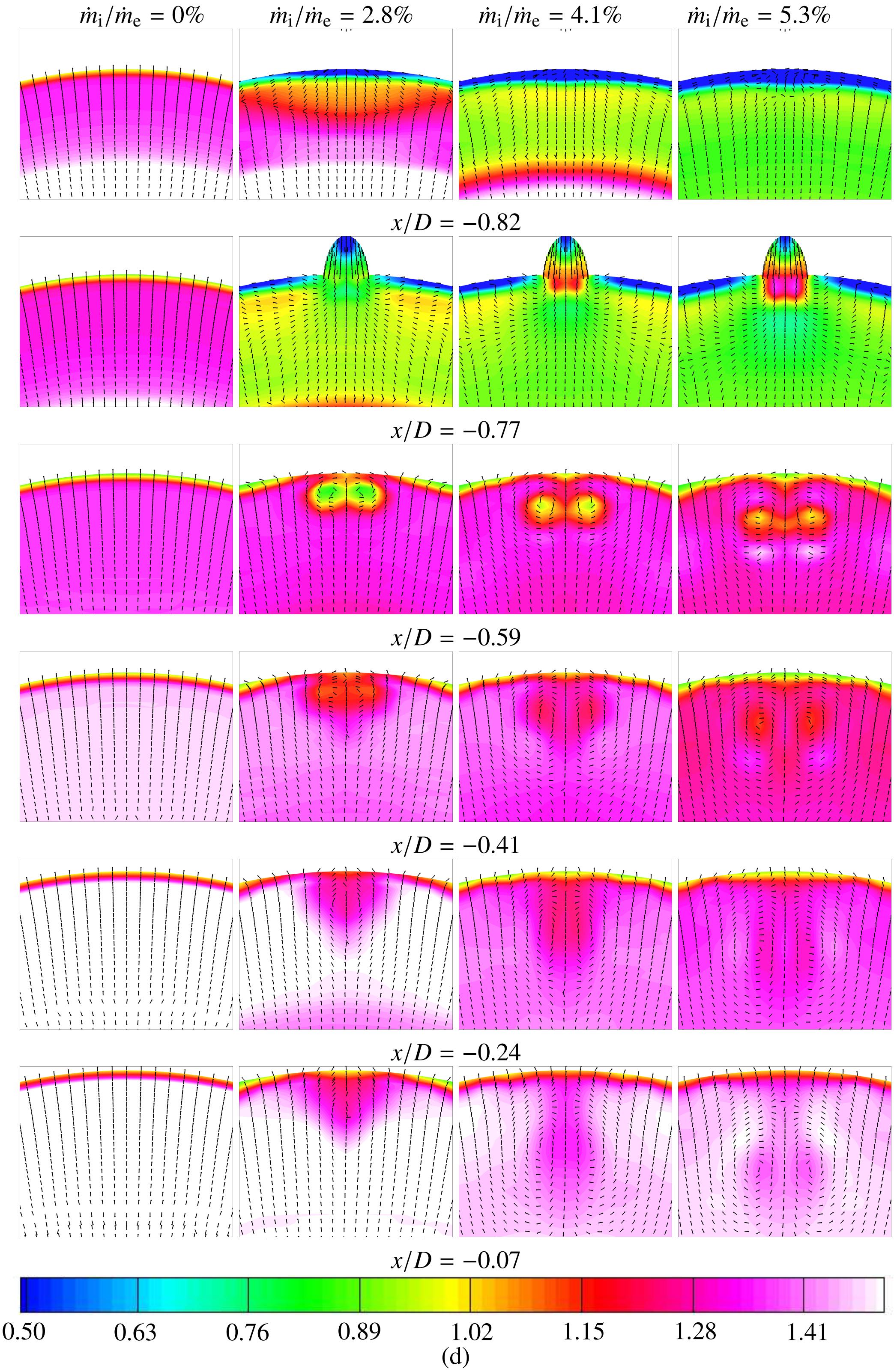

Figure 5.9: Time-averaged Mach number viewed at various $\hat{x}$-planes in the divergent sector of the nozzle illustrates the effect of injection mass flow on the mixing process.

5.2 Grid Refinement of the Baseline Case

To investigate the grid sensitivity of the flow field and the acoustics of the LES, the axial extent of the high resolution LES domain was doubled, as shown in Fig. 5.10. The average cell size in the axial direction in the high-resolution LES domain was also slightly decreased, as shown in Fig. 5.11. The finer cell size caused lower initial TKE downstream of the nozzle exit that results in increased TKE once the mixing process is initiated. Downstream of the original '2 to 1' interface, the TKE is higher, as expected, since the grid resolution is finer and hence allows more of the fine scale turbulence to be resolved. The increased turbulence in the shear layer increases mixing in the shear layer and results in reduced shock strength but still maintained shock spacing, as shown in Figs. 5.12-5.13. The increased turbulence results in increased noise for the downstream observers, as expected, as shown in Fig. 5.14. The screech frequency is unchanged, which indicates that the convective Mach number is still the same since the shock cell spacing is also unchanged. Interestingly, the magnitude of the screech is increased and the second harmonic can also be identified. However, the broadband shock associated noise is still of the same order of magnitude. A comparison of turbulent viscosity (μ_t) is shown in Fig. 5.15. The extension of the fine resolution area clearly impacts the magnitude of the turbulent viscosity, as expected.

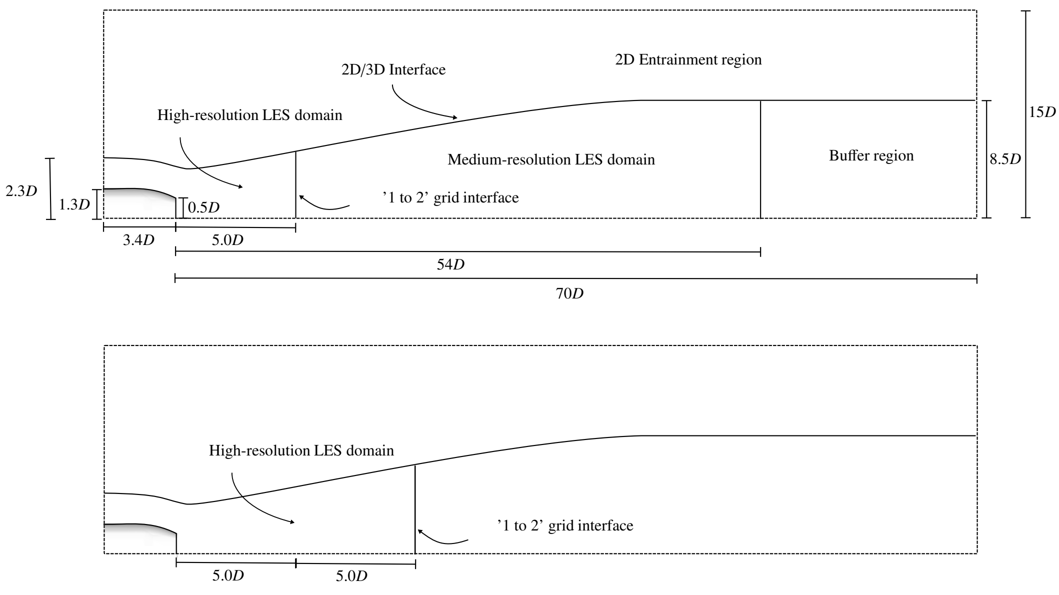

Figure 5.10: Schematic showing the increased size of the high resolution LES domain (bottom) compared to the original computational grid (top)

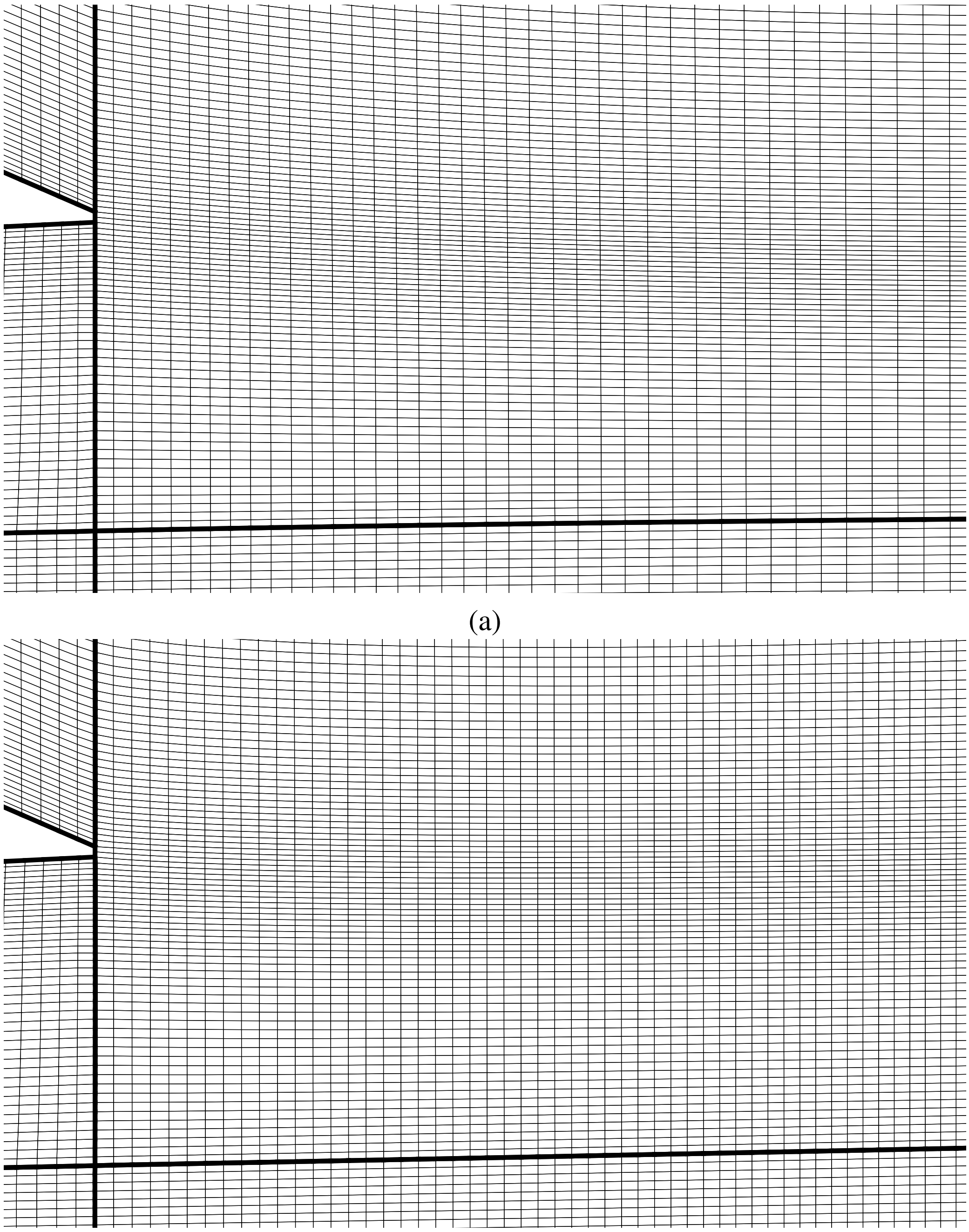

(a)

(b)

Figure 5.11: A zoom in on the nozzle exit: (a) Original grid (b) Refined grid. Note that the cell size in the radial direction is unchanged whereas it is smaller in the axial direction for the refined grid.

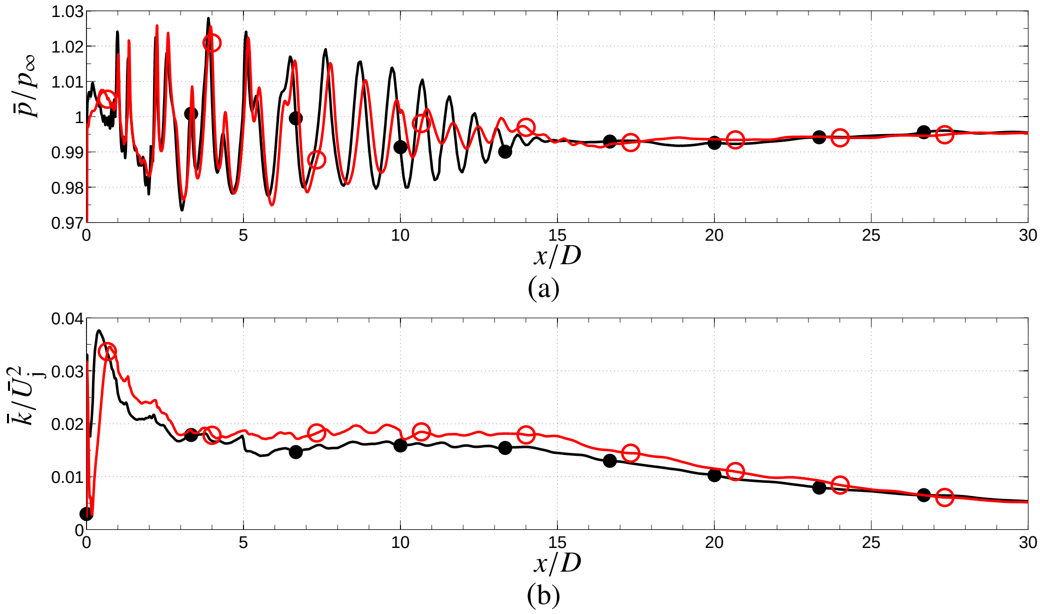

Figure 5.12: Flow profiles along the $\hat{x}$-axis at the radial location of $r/D = 0.5$, • Baseline grid, ◦ Refined grid.

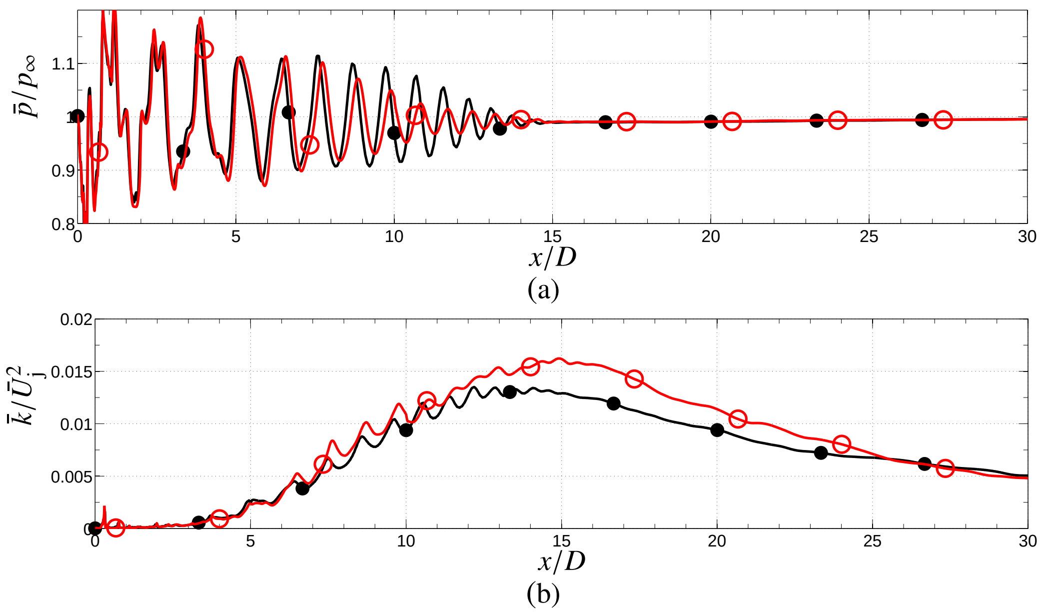

Figure 5.13: Flow profiles along $\hat{x}$-axis at radial location of $r/D = 0.25$, • Baseline grid, ◦ Refined grid.

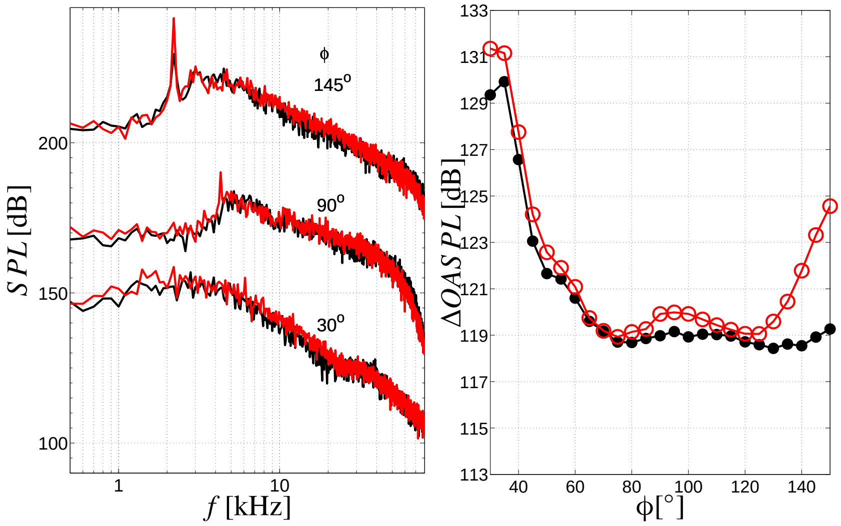

Figure 5.14: Far-fied acoustics for the • Baseline grid, ∘ Refined grid.

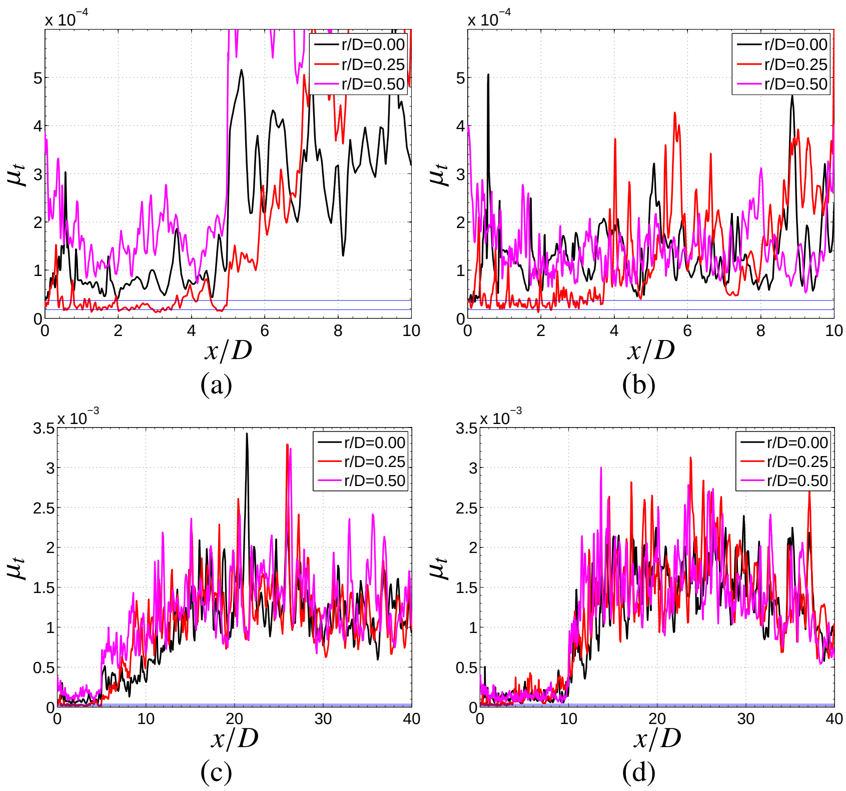

Figure 5.15: Comparison of turbulent viscosity (μ_t) of the baseline case and of the refined case. The laminar viscosity for two different temperatures, $\mu(T = 288\,\mathrm{K}) = 1.8 \cdot 10^{-5}\mathrm{kg/ms}$ and $\mu(T = 864\,\mathrm{K}) = 3.7 \cdot 10^{-5}\mathrm{kg/ms}$ is also plotted (blue).

Chapter 6

Concluding Remarks

The main findings of the work presented in the thesis are summarized as follows:

- The pulsed injection can achieve equal noise reduction as steady-state injection with less net mass flow. However, the pulsed injection increased the noise for the far-field observers in the downstream direction.

- The pulsed injection introduced pressure pulses that were radiated to the far-field. The pressure pulses were decreased by applying smooth sinusoidal pulsed injection, as compared to top-hat pulsed injection.

- The low frequency pulsed injection can be considered as quasi-steady state injection. The noise reduction of low frequency pulsed injection approaches the steady-state injection with increased modulation.

- Flapping injection was intended to reduce the pressure pulses that were found for the pulsed injection cases. This was thought to be achieved since it provides steady-state mass flow, while sinusoidally alternating the injection direction.

- Flapping injection did not result in improved noise reduction compared to the steady-state injection even though no or low pressure pulses were induced.

- Flapping injection may in some cases introduce large oscillations of the shock structure if the injection penetration is too large.

- 6 injectors were shown to be more efficient in mixing noise reduction than 12 injectors.

- Mixing noise was shown to decrease with increased injection mass flow for the investigated parameter space.

- Shock noise was shown to decrease to an optimum level with increased injection mass flow. Further mass flow injection resulted in increased shock noise.
- Spectral- and correlation study identified the screech tone both in the subsonic and supersonic regions of the jet.
- The jet was shown to exhibit a helical motion by using cross-correlations of pressure in the azimuthal direction at two radial locations within the subsonic and supersonic regions of the jet.
- Activated injection was shown to decrease the screech magnitude in the far-field to disrupt the helical motion of the jet and the onset of the screech in the jet plume. However, the helical motion picked up strength further downstream.
- Jet thrust is composed of two components: momentum thrust and pressure thrust at the nozzle exit. Fluidic injection is shown to decrease momentum thrust. Pressure thrust was increased because of shock displacement due to the injector shock interaction at the nozzle exit. The total thrust was increased, whereas the specific thrust was decreased with increased injection mass flow.
- The nozzle throat was optimized by Dr. Bernhard Gustafsson at GKN Aerospace in Trollhättan using RANS, with the objective of minimizing the strength of the shock attached to the nozzle throat and to provide even Mach number at the nozzle exit. Experiments and LES showed that the optimized design provided improved thrust without an acoustic penalty.
- The LES was found in general to be in good agreement with experiments. However:
  - LES fails to predict accurate locations of shocks for highly over-expanded cases due to premature separation in the divergent section of the nozzle.
  - The high frequency noise was in general slightly overpredicted by the LES for the steady injection cases.
- An increased jet temperature was found to result in increased noise radiation, in agreement with experimental data and results found in the literature. This is mainly due to increased jet exit velocity. The peak noise directivity was shown to shift to higher upstream angles with an increased jet temperature. The dominant noise sources were identified in the near-field.
- The Kirchhoff integral method did not predict accurate pressure skewness and pressure kurtosis in the far-field.

- The effect of jet viscosity on the flow-field and far-field acoustics was found to be insignificant at high temperatures.

6.1 Recommendations for future work

Although a vast amount of data was gathered, analyzed and presented in this thesis, there is still room for further research. A few of the topics of interest are listed here:

- Investigate injection into heated jets. The recent studies show that the LES accurately predicts the flow-field and far-field acoustics of the heated jets. It will be interesting to find out if the same shock noise breakdown and mixing noise reduction will be achieved.
- Investigate potential benefits of fluidic injection to the optimized nozzle.
- Investigate pulsed internal injection.
- Gather experimental near-field data to identify screech propagation and compare with LES.
- Conduct a correlation study in the jet core for other nozzle operation conditions to identify changes in screech propagation.
- Study engine performance with cycle analysis when extracting flow for fluidic injection from the compressor.
- Use improved wall model or use hybrid LES-RANS methods for future studies of over-expanded jet conditions.
- Investigate rectangular nozzles instead of circular nozzles. The flow physics of jets from rectangular nozzles are quite different than for jets from circular nozzles. They have been shown to mix more rapidly with a potential benefit for reduced noise reduction.

Bibliography

[1] Criteria for a recommended standard; Occupational Noise Exposure, 1998.

[2] S. James. Defining the cockpit noise hazard, aircrew hearing damage risk and the benefits active noise recuction headsets can provide. RTO-EN-HFM-111, 2004.

[3] H. Ising, E. Rebentisch, F. Poustka, and I. Curio. Annoyance and health risk caused by military low-altitude flight noise. *International Archieves of Occupational and Environmental Health*, 62:357–363, 1990.

[4] I. Holehouse. Sonic Fatigue of Aircraft Structures due to Jet Engine Fan Noise. *Journal of Sound and Vibration*, 17(3):287–298, 1971.

[5] B.L. Clarkson. Review of sonic fatigue technology. Technical report, April 1994.

[6] H. Hubbard and D. Maglieri. Sonic Fatigue of Aircraft Structures due to Jet Engine Fan Noise. *Journal of Sound and Vibration*, 43(2):159–172, 1975.

[7] Making Future Commercial Aircraft Quieter. *NASA Facts*, July 1999.

[8] S.C. Crow and F.H. Champagne. Orderly structure in jet turbulence. *Journal of Fluid Mechanics*, 48(03):547–591, 2006.

[9] M.J. Lighthill. On sound generated aerodynamically, I. General theory. *Proc. Roy. Soc.*, A 211:564–587, 1952.

[10] J. E. Ffowcs Williams. The noise from turbulence convected at high speed. *Philosophical Transactions of the Royal Society of London. Series A: Mathematical, Physical and Engineering Sciences*, 255(1061):469–503, 1963.

[11] M. Smith. *Aircraft noise*. Cambridge University Press, 1st edition, 1989. ISBN 0-521-33186-2.

[12] C.K.W. Tam. Jet noise: Since 1952[1]. *Theoret. Comput. Fluid Dynamics*, 10:393–405, 1998.

[13] J. Atvars, L.K. Schubert, and H.S. Ribner. Refraction of sound from a point source placed in an air jet. *Journal of the Acoustical Society of America*, 37(1):168–170, 1965.

[14] C.K.W. Tam. Supersonic jet noise. *Annu. Rew. Fluid Mech.*, 27:17–43, 1995.

[15] C.K.W. Tam and H.K. Tanna. Shock associated noise of supersonic jets from convergent-divergent nozzles. *Journal of Sound and Vibration*, 81(3):337 – 358, 1982.

[16] M. Harper-Bourne and M.J. Fisher. The noise from shock waves in supersonic jets. In *AGARD Conference proceedings no 131 on Noise mechanisms*, number AGARD-CP-131 :1-13, 1973.

[17] C.K.W. Tam. Jet noise generated by large-scale coherent motion. In H.H. Hubbard, editor, *Aeroacoustics of Flight Vehicles, Theory and Practice, Volume 1: Noise Sources*. Acoustical Society of America, Woodbury, NY, 1995.

[18] A. Powell. The Noise of Choked Jets. 25(3):385–389, 1953.

[19] B. Henderson. Fifty years of fluidic injection for jet noise reduction. *International Journal of Aeroacoustics*, 9(1 and 2):91–122, 2010.

[20] N. Chauvet, S. Deck, and L. Jacquin. Numerical Study of Mixing Enhancement in a Supersonic Round Jet. *AIAA Journal*, 45(7):1675–1687, July 2007.

[21] M. Aberg, R.-Z. Szasz, L. Fuchs, and E. Gutmark. Numerical Study of Fluidic Injection for Noise Reduction. In *45th AIAA Aerospace Sciences Meeting and Exhibit*, Aerospace Sciences Meetings. American Institute of Aeronautics and Astronautics, January 2007.

[22] J.B. Freund and P. Moin. Jet Mixing Enhancement by High-Amplitude Fluidic Actuation. *AIAA Journal*, 38(10):1863–1870, October 2000.

[23] S. Lardeau, E. Lamballais, and J.-P. Bonnet. Direct numerical simulation of a jet controlled by fluid injection. *Journal of Turbulence*, 3(917396936):N2, January 2002.

[24] M.K. Ibrahim, R. Kunimura, and Y. Nakamura. Mixing enhancement of compressible jets by using unsteady microjets as actuators. *AIAA Journal*, 40(4):681–688, 2002.

[25] C. Chenault, J. Dorri, D. Smith, and V. Kibens. Active core exhaust (ACE) control for reduction of thermal loading. In *Fluids 2000 Conference and Exhibit*, Fluid Dynamics and Co-located Conferences. American Institute of Aeronautics and Astronautics, June 2000.

[26] G. Raman and A.B. Cain. Innovative actuators for active flow and noise control. *Journal of Aerospace Engineering*, 216(6):303–324, 2002.

[27] P. Ragaller, A. Annaswamy, B. Greska, and A. Krothapalli. Supersonic jet noise reduction via pulsed microjet injection. In *The 15th AIAA/CEAS Aeroacoustics Conference*, number AIAA-2009-3224, Miami, Florida, 2009.

[28] M. Huet, B. Fayard, G. Rahier, and F. Vuillot. Numerical Investigation of the Micro-Jets Efficiency for Jet Noise Reduction. In *15th AIAA/CEAS Aeroacoustics Conference (30th AIAA Aeroacoustics Conference)*, Aeroacoustics Conferences. American Institute of Aeronautics and Astronautics, May 2009.

[29] G.D. Roy. *Combustion Process in Propulsion*, chapter Chapter 3. Butterworth-Heinemann Ltd, 1st edition, 2005. ISBN10: 0123693942.

[30] M. Kearney-Fishcer, J.H. Kim, and M. Samimy. Noise control of a high reynolds number mach 0.9 heated jet using plasma actuators. In *15th AIAA/CEAS Aeroacoustics Conference*, number AIAA-2009-3188, Miami, Florida, 2010.

[31] J.H. Kim, M. Nishihara, I.V. Adamovich, M. Samimy, S.V. Gorbatov, and F.V. Pliavaka. Development of localised arc filament rf plasma actuators for high-speed and high reynolds number flow control. *Exp Fluids*, 49:497–511, 2010.

[32] A. Sinha, K. Kim, J.H. Kim, A. Serrani, and M. Samimy. Extremizing feedback control of a high-speed and high reynolds number jet. *AIAA Journal*, 48(2):387–399, 2010.

[33] M. Samimy, J.H. Kim, and M. Kearney-Fishcer. Active control of noise in supersonic jets using plasma actuators. In *ASME Turbo Expo 2009*, GT2009-59456, Orlando, Florida, 2009.

[34] M. Kearney-Fishcer and M. Samimy. Noise control of a high reynolds number mach 1.3 heated jet using plasma actuators. In *48th AIAA Aerospace Sciences Meeting*, number AIAA-2010-13, Orlando, Florida, 2010.

[35] M. Samimy, J.H. Kim, M. Kearney-Fischer, and A. Sinha. Acoustic and flow fields of an excited high reynolds number axisymmetric supersonic jet. *Journal of Fluid Mechanics*, 656:507–529, 2010.

[36] D.V. Gaitonde and M. Samimy. Effect of plasma-based azimuthal mode excitation on supersonic jet flow. In *5th Flow Control Conference*, number AIAA-2010-4416, Chicaco, Illinois, 2010.

[37] A. Ben-Yakar, M. G. Mungal, and R. K. Hanson. Time evolution and mixing characteristics of hydrogen and ethylene transverse jets in supersonic crossflows. *Physics of Fluids (1994-present)*, 18(2):–, 2006.

[38] B. Gustafsson. *Eperimental Studies of Effusion Cooling*. PhD thesis, Division of Thermo and Fluid Dynamics, Chalmers University of Technology, Gothenburg, 2001. ISBN 91-7291-028-3.

[39] B. Semlitsch, M. Mihaescu, E. Gutmark, and L. Fuchs. Flow structure generation by multiple jets in supersonic cross-flow. In *4th International Conference on Jets, Wakes and Separated Flows*, number ICJWSF2013-1178, Nagoya, Japan, 2013.

[40] D. Cuppoletti. *Supersonic Jet Noise Reduction with Novel Fluidic Injection Techniques*. PhD thesis, University of Cincinnati, 2013.

[41] M.R. Gruber, A.S. Nejadt, T.H. Chen, and J.C. Dutton. Mixing and Penetration Studies of Sonic Jets in a Mach 2 Freestream. *Journal of Propulsion and Power*, 11(2):315–323, March 1995.

[42] E. Gutmark, I.M. Ibrahim, and S. Murugappan. Circular and noncircular subsonic jets in cross flow. *Physics of Fluids (1994-present)*, 20(7):–, 2008.

[43] J. Smagorinsky. General circulation experiment with the primitive equations. I. The basic experiment. *Monthly Weather Review*, 91(3):99–165, 1963.

[44] G. Erlebacher, M. Y. Hussaini, C. G. Speziale, and T. A. Zang. Toward the large-eddy simulation of compressible turbulent flows. *Journal of Fluid Mechanics*, 238:155–185, 1992.

[45] N. Andersson. *A Study of Subsonic Turbulent Jets and Their Radiated Sound Using Large-Eddy Simulation*. PhD thesis, Division of Fluid Dynamics, Chalmers University of Technology, Gothenburg, 2005. ISBN 91-7291-679-6.

[46] M. Burak. *Large Eddy Simulation for the Analysis of Supersonic Jet Noise Suppression Devices*. PhD thesis, Division of Fluid Dynamics, Chalmers University of Technology, Gothenburg, 2010. ISBN 978-91-7385-459-7.

[47] L.-E. Eriksson. Development and validation of highly modular flow solver versions in g2dflow and g3dflow. Internal report 9970-1162, Volvo Aero Corporation, Sweden, 1995.

[48] H. Mårtensson, L.-E. Eriksson, and P.J. Albråten. Numerical simulations of unsteady wakeflow. Nottingham, United Kingdom, 1991. The 10th ISABE meeting.

[49] C. Wollblad. *Transonic flow: large eddy simulation, numerical methods and subgrid modeling*. PhD thesis, Division of Fluid Dynamics, Chalmers University of Technology, Gothenburg, 2006.

[50] L.-E. Eriksson. Compressible CFD and CAA. Lecture notes, Division of Thermo and Fluid Dynamics, Chalmers University of Technology, Gothenburg, Sweden, 2006.

[51] M. Perrino, D. Munday, E. Gutmark, M. Burak, and L. E. Eriksson. Microjet flow control for noise reduction of a supersonic jet from a practical c-d nozzle. Stockholm, Sweden, 2010. 16th AIAA/CEAS Aeroacoustics Conference.

[52] D. Munday, N. Heeb, M. Perrino, E. Gutmark, M.O.Burak, L.-E. Eriksson, and E. Prisell. Comparison of flow control methods applied to conical c-d nozzles. In *The 16th AIAA/CEAS Aeroacoustics Conference*, number AIAA-2010-3874, Stockholm, Sweden, 2010.

[53] D. Cuppoletti, M. Perrino, and E. Gutmark. Fluid injection effects on acoustics of a supersonic jet at various mach numbers. Portland, Oregon, 2011. The 17th AIAA/CEAS Aeroacoustic Conference.

[54] M. Samimy, J.-H. Kim, J. Kastner, I. Adamovich, and Y. Utkin. Active control of high-speed and high-reynolds-number jets using plasma actuators. *Journal of Fluid Mechanics*, 578:305–330, 2007.

[55] M. Samimy, J.-H. Kim, J. Kastner, I. Adamovich, and Y. Utkin. Active control of a mach 0.9 jet for noise mitigation using plasma actuators. *AIAA Journal*, 45(4):890–901, 2007.

[56] D. Cuppoletti, E. Gutmark, H. Hafsteinsson, L.-E. Eriksson, and E. Prisell. A Comprehensive Investigation of Pulsed Fluidic Injection for Active Control of Supersonic Jet Noise. In *51st AIAA Aerospace Sciences Meeting including the New Horizons Forum and Aerospace Exposition*, Aerospace Sciences Meetings. American Institute of Aeronautics and Astronautics, January 2013.

[57] A. Powell. On the mechanism of choked jet noise. *Proceedings of the Physical Society. Section B*, 66(12):1039, 1953.

[58] R. Larusson, H.E. Hafsteinsson, N. Andersson, and L.-E. Eriksson. Investigation of Supersonic Jet Flow Using Modal Decomposition. In *20th AIAA/CEAS Aeroacoustics Conference*, AIAA Aviation. American Institute of Aeronautics and Astronautics, June 2014.

[59] Y. Saad. *Iterative Methods for Sparse Linear Systems*. Society for Industrial and Applied Mathematics, second edition, 2003.

[60] J.H. Tu, C.W. Rowley, D.M. Luchtenburg, S.L. Brunton, and J.N. Kutz. On Dynamic Mode Decomposition: Theory and Applications. *ArXiv e-prints*, November 2013.

[61] J.E.F. Williams, J. Simson, and V.J. Virchis. Crackle: an annoying component of jet noise. *Journal of Fluid Mechanics*, 71(02):251, March 2006.

[62] C. Bogey and C. Bailly. Effects on inflow conditions and forcing on subsonic jet flows and noise. *AIAA Journal*, 43(5):1000–1007, 2005.

[63] P. J. Morris. The spatial viscous instability of axisymmetric jets. *Journal of Fluid Mechanics*, 77:511–529, October 1976.

[64] J. Liu, K. Kailasanath, R. Ramamurti, D. Munday, E. Gutmark, and R. Lohner. Large-Eddy Simulations of a Supersonic Jet and Its Near-Field Acoustic Properties. *AIAA Journal*, 47(8):1849–1865, August 2009.